EXPLORING NEW PHYSICS BELOW AND ABOVE THE ELECTROWEAK SCALE

A THESIS SUBMITTED TO
THE GRADUATE SCHOOL OF NATURAL AND APPLIED SCIENCES
OF
MIDDLE EAST TECHNICAL UNIVERSITY

BY

ESRA AKYUMUK

IN PARTIAL FULFILLMENT OF THE REQUIREMENTS
FOR
THE DEGREE OF MASTER OF SCIENCE
IN
PHYSICS

SEPTEMBER 2022

Approval of the thesis:

EXPLORING NEW PHYSICS BELOW AND ABOVE THE ELECTROWEAK SCALE

submitted by **ESRA AKYUMUK** in partial fulfillment of the requirements for the degree of **Master of Science in Physics Department, Middle East Technical University** by,

Prof. Dr. Halil Kalıpçılar
Dean, Graduate School of **Natural and Applied Sciences** _____

Prof. Dr. Seçkin Kürkçüoğlu
Head of Department, **Physics** _____

Prof. Dr. İsmail Turan
Supervisor, **Physics, METU** _____

Assist. Prof. Dr. Durmuş Karabacak
Co-supervisor, **Energy Systems Engineering, MSKU** _____

Examining Committee Members:

Prof. Dr. İnanç Şahin
Physics, Ankara University _____

Prof. Dr. İsmail Turan
Physics, METU _____

Assoc. Prof. Dr. Levent Selbuz
Engineering Physics, Ankara University _____

Assoc. Prof. Dr. İsmet Yurduşen
Mathematics, Hacettepe University _____

Assist. Prof. Dr. Durmuş Karabacak
Energy Systems Engineering, MSKU _____

Date: 01.09.2022

I hereby declare that all information in this document has been obtained and presented in accordance with academic rules and ethical conduct. I also declare that, as required by these rules and conduct, I have fully cited and referenced all material and results that are not original to this work.

Name, Surname: Esra Akyumuk

Signature :

ABSTRACT

EXPLORING NEW PHYSICS BELOW AND ABOVE THE ELECTROWEAK SCALE

Akyumuk, Esra
M.S., Department of Physics
Supervisor: Prof. Dr. İsmail Turan
Co-Supervisor: Assist. Prof. Dr. Durmuş Karabacak

September 2022, 63 pages

There are new physics scenarios which are intended to modify the Standard Model either at low or high energy scales. The interaction of a so-called hidden sector with the Standard Model through various portals can be visualized at low energies, which can be explored by using the data from fixed target experiments, beam dumped experiments etc. Vector portal is one venue to explore the hidden sector through coupling with the Standard Model. One way to visualize vector portal effects would be neutrino charge radius. Furthermore, recent successful measurement of the coherent neutrino nucleus cross section could also be sensitive to the electromagnetic form factors of neutrino. Therefore, together with the vector portal contribution to the neutrino electromagnetic form factors, specifically, the magnetic moment and charge radius of neutrino will be discussed. On the other hand, new physics has been traditionally investigated in the framework of various scenarios at high energies beyond the validity of the Standard Model. One such scenario would be the so-called Fat-brane Universal Extra Dimension Model whose signals can be tested at the Large Hadron Collider (LHC). The colored level-1 KK (Kaluza-Klein) particles can be pair-produced at the

LHC. From the cascade decays of these particles, dijet plus missing transverse energy signal and photonic signal topologies can be expected. The ATLAS Collaboration recently has reported two searches at 13 TeV center-of-mass energy and 139 inverse femtobarn integrated luminosity data; multi-jet plus missing transverse energy and photon-j plus missing transverse energy. In the absence of excess events in both searches, the fundamental parameters of fat-brane UED model, namely, the extra dimensional Planck mass (M_D) and the size of the small extra dimension (R^{-1}) will be constrained.

Keywords: Physics beyond standard model, neutrino charge radius, phenomenology of the field theories in higher dimensions, Extra-dimensional scenarios

ÖZ

YENİ FİZİĞİN ELEKTROZAYIF ÖLÇEĞİN ALTINDA VE ÜSTÜNDE ARAŞTIRILMASI

Akyumuk, Esra
Yüksek Lisans, Fizik Bölümü
Tez Yöneticisi: Prof. Dr. İsmail Turan
Ortak Tez Yöneticisi: Dr. Öğr. Üyesi. Durmuş Karabacak

Eylül 2022 , 63 sayfa

Standart Modeli düşük veya yüksek enerji ölçeklerinde değiştirmeyi amaçlayan yeni fizik senaryoları vardır. Gizli sektörün çeşitli portallar aracılığıyla Standart Model ile etkileşimi, düşük enerjilerde gerçekleşebilir ve bu etkileşimler sabit hedef, ışın dökümlü deneyleri gibi deney verileri ile incelenebilir. Vektör portalı, Standart Model ile etkileşime girerek gizli sektörün keşfedilebileceği bir alandır. Vektör portal etkilerini görebilmenin bir yolu, nötrino yük yarıçapı olacaktır. Öte yandan, elastik nötrino-çekirdek tesir kesitinin son zamanlardaki başarılı ölçümü, nötrinonun elektromanyetik form faktörlerine de duyarlı olabilir. Bu nedenle, nötrino elektromanyetik form faktörlerine vektör portal katkısı ile birlikte, özel olarak nötrinonun manyetik momenti ve yük yarıçapı tartışılacaktır. Öte yandan yeni fizik, geleneksel olarak Standart Modelin geçerliliğini aşan yüksek enerjilerde çeşitli senaryolar çerçevesinde araştırılmıştır. Böyle bir senaryo, sinyalleri şu anda çalışmakta olan Büyük Hadron Çarpıştırıcısında (LHC) test edilebilen Kalın-zar Evrensel Ekstra Boyut Modeli olabilir. Renkli seviye-1 KK (Kaluza-Klein) parçacıkları LHCde çiftler halinde üretile-

bilir. Bu parçacıkların kademeli bozunmalarından, dijet artı kayıp transverse enerji sinyali ve fotonik sinyal topolojileri beklenebilir. ATLAS İşbirliği yakın zamanda 13 TeV kütle merkezi enerjisi ve 139 ters femtobarn verisinde iki araştırma rapor etmiştir; çoklu jet artı kayıp transverse enerji ve foton-j artı kayıp transverse enerji. Her iki aramada da fazla olayın olmaması durumunda, kalın-zar UED modelinin temel parametreleri, yani ekstra boyutlu Planck kütlesi (M_D) ve küçük ekstra boyutun boyutu (R^{-1}) sınırlandırılacaktır.

Anahtar Kelimeler: Standart model ötesi fizik, nötrino yük yarıçapı, evrensel ekstra boyutlarda alan teorileri fenomenolojisi, ekstra boyut senaryoları

To My Family

ACKNOWLEDGMENTS

First and foremost, I would like to express my sincere gratitude to my supervisor Prof. Dr. İsmail Turan for his expertise, knowledge and unlimited support throughout my master's study.

I would like to also thank my co-supervisor Dr. Durmuş Karabacak for his patience and support which helped me to learn new tools which were not familiar to me.

I am grateful to Prof. Dr. T. Aliyev for the discussions about the neutrino physics during coffee breaks, both of which helped me a lot.

Lastly, I want to express my deepest gratitude to my love Alperen, he was always on my side and helping me to cope with the problems I have been facing with patience. I also want to thank Vivi Karoo, my beautiful little cutie.

This work is supported in part by TÜBITAK through 118F390 and 121F051.

TABLE OF CONTENTS

LIST OF TABLES

TABLES

LIST OF FIGURES

FIGURES

LIST OF ABBREVIATIONS

SM	Standard Model
LHC	Large Hadron Collider
SUSY	Supersymmetry
ADD	Arkani-Dimopoulos-Dvali Model
UED	Universal Extra Dimensions
KK	Kaluza-Klein
GMD	Gravity Mediated Decay
KKCD	KK-number Conserving Decay
LKP	Lightest Kaluza-Klein Particle
BSM	Beyond Standard Model
CP	Charge Conjugation Parity
CL	Confidence Level

CHAPTER 1

INTRODUCTION

After the discovery of the Higgs boson [1, 2], which is the last needed fundamental particle of the Standard Model (SM) of particle physics [3], the particle spectrum of the Standard Model has completed. Over the past decade, results from the LHC also show that the Standard Model agrees tremendously with the observational data [4].

On the other hand, the instability of the mass of the Higgs boson under ultraviolet corrections (naturalness problem) [5–7], the mass of neutrinos [8], and the presence of dark matter [9] are the subjects that do not have an explanation in the Standard Model. The physicists have been developing new physics models that can answer these problems while preserving the symmetries of the SM.

New physics models can be searched in either side of the electroweak scale. In the low energy region, the hidden sector is one venue to explain the problems and anomalies of the SM. The reason that this sector is 'hidden' (or 'dark') is that the interaction of the SM with this sector is assumed to be very weak. The interaction of the dark sector and visible sector (SM) occurs via mediator particles which are both charged under the dark sector and the visible sector and they act as a 'portal' between two sectors. The interaction of the mediator particles with the SM particles can be direct or indirect, depending on the model. The portals that connect the SM to the dark sector can be mainly categorized into four: neutrino portal, Higgs portal, axion portal, and vector portal. The mediator particles can be scalars ϕ, pseudoscalar a, vector A', axial vector Z', and fermions N. In this thesis, the vector portal (whose mediator is named as the dark photon A') will be the main focus of the new physics searches on the low energy region of the electroweak scale.

Other theoretical structures that can answer the current problems of SM are built on multiple space-time models. For example, in the Arkani-Dimopoulos-Dvali (ADD) model [10, 11], elementary particles are placed on the brane (3-brane), and only gravitation is assumed to reach N large extra dimensions ($\sim eV^{-1}$ to keV^{-1}). As a result of this structure, the Planck mass in 4D is reduced by the volume from the extra dimensions, and the high-dimensional Planck mass (M_D) is in the order of a few TeV, thus solving the naturalness problem of the SM. In the case of the ADD model, the results of the ATLAS group on the $139\ fb^{-1}$ dataset and the missing transverse energy and mono-jet signal at the centre of mass energy of 13 TeV; for $N = 2$, $M_D = 11.2\ TeV$, and $N = 6$, $M_D = 5.9\ TeV$ at 95% confidence level (CL) limits have been introduced [12]. Another multi-dimensional space-time model is the Randall-Sundrum (RS) model [13, 14], which is a higher-dimensional warped metric space-time model with two different brane structures (in the RS-I version of the model, there are two separate branes in the TeV and Planck mass energy orders) is trying to explain the naturalness problem of the SM. The current limits of the model for the RS-I variant can be found in [15].

Another model among the multi-dimensional space-time models that can be observed in the current collider experiments is the Universal Extra Dimensions (UED) [16–18]. Although the UED models do not solve the naturalness problem as neatly as in the ADD and RS models, they rather introduce a new mechanism for spontaneous breaking of SUSY [16], relaxing the upper limit of the mass of the lightest uncharged Supersymmetric Higgs boson [19], lowering the unification scale down to a few TeV orders [20–23]. In addition to being able to bring a new aspect to the mass hierarchy of fermions [24], predict that the number of the generation of fermions should be three or a multiple of three [25], and contain a cosmologically suitable cold dark matter candidate [26–37], the UED models also draw attention by presenting compelling the rich collider physics [33].

The minimal UED (mUED), the most constrained version of the model, is created by adding a single extra dimension relatively small in length and compacted on a circle to (3+1)d dimensional space-time while preserving the gauge symmetry of the SM. Considering the elements of the mUED model, such as KK symmetry and particle spectrum, it can be seen that it is similar to the SUSY models in which R-parity is

conserved [38]. 'Fat-Brane' UED model is a variant of the mUED model obtained by embedding the space-time structure in the mUED on the 4+N dimensional bulk, under the assumption of N large extra dimensions (in the range of $\sim eV^{-1} - keV^{-1}$) that only gravity can reach. In this thesis, the fat-brane mUED model will be the main focus of the new physics searches on the high energy region of the electroweak scale.

CHAPTER 2

VECTOR PORTAL CONTRIBUTION TO THE NEUTRINO ELECTROMAGNETIC FORM FACTORS

2.1 Electromagnetic Properties of Neutrino

The neutrino and its electromagnetic properties have been an exciting and active research area in particle physics. In the Standard Model, neutrinos are weakly interacting massless left-handed fermions. It means that the electromagnetic characteristics of a neutrino are all zero. However, the discovery of neutrino oscillations proved that neutrinos are massive particles, and this discovery can reasonably support the non-zero electromagnetic properties of neutrinos and leads scientists to explore the properties and interactions of the neutrinos beyond the Standard Model (BSM). The study of electromagnetic properties of neutrinos beyond the Standard Model can constrain the existing BSM scenarios and give a clue about new physics.

In favour of the existence of neutrino charge radius, participation of the neutrinos in electromagnetic interactions can be expected to be observed in the nearest future. The knowledge of the value of the neutrino charge radius would not be enough to determine the electromagnetic properties of neutrinos. It would be great to discover whether the neutrino charge radius is strictly diagonal with respect to the neutrino flavour or not. If the neutrino charge radius is not diagonal with respect to the neutrino flavour, that will indicate a new physics beyond the SM since it does not allow any change of neutrino flavour as a result of interactions of neutrino. The other electromagnetic properties of neutrinos are electric charge (milicharge), magnetic moment, anapole moment and electric dipole moment. Theoretical aspects of the main characteristics of electromagnetic properties of neutrino and their current experimental

limits will be discussed in the next section.

In this study, neutrino charge radius will be investigated under the $U_{B-L}(1)$ model.

2.1.1 Electromagnetic Vertex Function of Neutrino

The neutrino does not electromagnetically interact with matter at the tree level because it is electrically neutral. However, electromagnetic interactions can occur radiatively.

The effective Hamiltonian of the electromagnetic interaction of a Dirac neutrino, in one photon limit, can be defined as;

$$\mathcal{H}_{\rm em}(x) = j_{\mu}^{EM}(x)A^{\mu}(x) = \overline{\nu_f}(x)\Lambda_{\mu}\nu_i(x)A^{\mu}(x) \tag{2.1}$$

where Λ_{μ} is the electromagnetic vertex function and $j_{\mu}^{EM}(x)$ is the electromagnetic current. Λ_{μ} is the definition of the matrix element whose description is the transition of an initial state Dirac neutrino ν_i, and a final state neutrino ν_f with an initial momentum p_i and final momentum p_f, respectively (Figure 2.1).

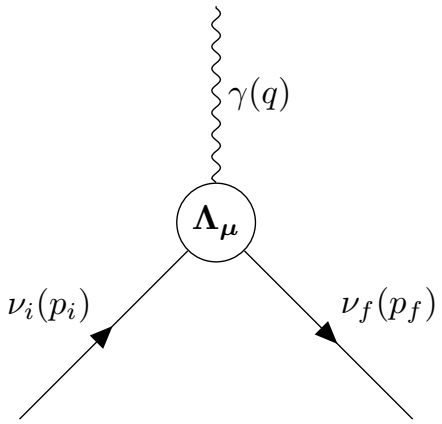

Figure 2.1: The effective vertex of the electromagnetic interaction of the neutrino.

Consistent with the Lorentz and electromagnetic gauge invariance, the most general form of the electromagnetic vertex function Λ_{μ} is defined as,

$$\Lambda_\mu(q) = f_Q\left(q^2\right)\gamma_\mu + f_E\left(q^2\right)\sigma_{\mu\nu}q^\nu\gamma_5 - f_M\left(q^2\right)i\sigma_{\mu\nu}q^\nu + f_A\left(q^2\right)\left(q^2\gamma_\mu - q_\mu \not{q}\right)\gamma_5 \tag{2.2}$$

In this formulation, there is no possible transition between neutrino flavours. With the interaction of a real photon ($q^2 = 0$), the four sets of the neutrino electromagnetic form factors $f_{Q,E,M,A}$ are the electric charge, electric dipole moment, magnetic dipole moment and anapole moment.

2.1.2 Electric and Magnetic Dipole Moments of Neutrino

The starting point of the investigation of neutrino electromagnetic properties is after it was shown that for a massive neutrino, in the extended Standard Model with right-handed neutrinos, the magnetic moment is a non-vanishing quantity, and its value is determined by the mass of the neutrino [39–44]. Among the electromagnetic properties of the neutrino, magnetic and electric dipole moments are the ones that are being studied mainly since they naturally emerge from the extensions of the SM. For a Dirac neutrino, in the minimal extension of the Standard Model, magnetic moment, which is diagonal in the mass basis, has a form [41],

$$\mu_{ii}^D = \frac{3eG_F m_i}{8\sqrt{2}\pi^2} \approx 3.2 \times 10^{-19}\left(\frac{m_i}{1\mathrm{eV}}\right)\mu_B \tag{2.3}$$

where μ_B is Bohr magneton.

For a Majorana neutrino, the magnetic moment has a non-diagonal form in the mass basis, which allows only transition magnetic moments.

The most general and model-independent upper limits for the magnetic moment of a Dirac neutrino, generated above the electroweak symmetry breaking scale, within the current bound on neutrino mass implies that neutrino magnetic moment is around $|\mu_0| < 10^{-14}\ \mu_B$ [45]. Compared to the bounds from astrophysical observations and solar and reactor neutrino data, this bound is stronger by several orders of magnitude. The corresponding upper limit for the magnetic moment of the Majorana neutrino is much weaker [46].

For a Dirac neutrino, at zero momentum transfer, the diagonal type of electric dipole moment vanishes due to the hermicity of the electromagnetic current and the assumption of its invariance under CP transformation. Nonzero electric dipole moments occur only in the models where CP symmetry is violated. Astrophysical and laboratory experiments where contributions of magnetic moments in neutrino scattering are examined can also provide constraints on the electric dipole moments since the contributions from electric dipole moments interfere with the contributions from magnetic dipole moments [47–49].

2.1.3 Neutrino Charge Radius

It is known that neutrino, as in the name suggests, is a neutral particle. However, neutrino electric properties can still be obtained from the electric form factor f_Q. It is possible to characterize a neutral particle as a superposition of two different charge distributions with opposite signs. This is defined by the electric form factor which is non-zero for $q^2 = 0$.

Expand the electric charge form factor in series around $q^2 = 0$,

$$f_Q\left(q^2\right) = f_Q(0) + q^2 \frac{df_Q\left(q^2\right)}{dq^2}\bigg|_{q^2=0} + \ldots \tag{2.4}$$

The first term is the electric charge of the neutrino, and the second term gives the neutrino charge radius.

Consider a spherically symmetric charge distribution with charge density $\rho(r)$; the charge form factor can be interpreted as a Fourier transformation of $\rho(r)$, in the so-called Breit frame where $q_0 = 0$. In this frame, charge form factor only depends on $|\vec{q}| = \sqrt{-q^2}$ with $r = |\vec{x}|$,

$$f_Q\left(q^2\right) = \int \rho(r) e^{-i\vec{q}\cdot\vec{x}} d^3x = \int \rho(r) \frac{\sin(|\vec{q}|r)}{|\vec{q}|r} d^3x \tag{2.5}$$

Taking the first derivative of this expression with respect to $q^2 = -|\vec{q}|^2$,

$$\frac{df_Q\left(q^2\right)}{dq^2} = \int \rho(r) \frac{\sin(|\vec{q}|r) - |\vec{q}|r\cos(|\vec{q}|r)}{2q^3 r} d^3x \tag{2.6}$$

is obtained and,

$$\lim_{q^2\to 0} \frac{df_Q\left(q^2\right)}{dq^2} = \int \rho(r) \frac{r^2}{6} d^3x = \frac{\langle r^2 \rangle}{6} \tag{2.7}$$

Therefore, the squared charge radius of neutrino is defined as,

$$\left\langle r^2 \right\rangle = 6 \frac{df_Q\left(q^2\right)}{dq^2}\bigg|_{q^2=0} \tag{2.8}$$

It should be noted that since the charge density $\rho(r)$ is not defined as a positive quantity, $\langle r^2 \rangle$ can be negative.

It is convenient to summarise the controversial history of the neutrino charge radius in the Standard Model in the following.

First, it was claimed that neutrino charge radius is not a physical quantity in the Standard Model in the unitary gauge since the result is ultraviolet divergent [50]. For a massive Dirac neutrino, a direct one-loop calculation of $\gamma - Z$ self-energy diagrams and proper vertices in a general R_ξ gauge also gave a divergent result if $q^2 \neq 0$ [51]. However, by introducing the contributions from neutrino-lepton neutral scattering diagrams to the usual terms, it is possible to obtain a finite but gauge-dependent result for the neutrino charge radius in unitary gauge [52]. Afterwards, it was shown that it is possible to obtain a finite and gauge independent value for the neutrino charge radius by considering additional box diagrams with the contributions from the proper diagrams [40], and this leads to the discussion of neutrino electroweak radius which was defined by [53, 54]. In [55], an additional set of diagrams that contribute to the electroweak radius of the neutrino was discussed. Finally, the neutrino electroweak radius was introduced as a physical observable by [56–58]. The corresponding calculations are performed while including the box diagrams involving W-Z bosons and additional terms from the $\gamma - Z$ boson mixing in the one-loop approximation, and a gauge-invariant result has been obtained for the neutrino charge radius. However, this

result leads to revivifying the discussion about the definition of the neutrino charge radius [59–62].

In this thesis, the contribution of the dark photon to the one-loop calculation of the neutrino charge radius is calculated in the Feynman gauge. Contributory diagrams are called proper vertices, $\gamma - Z$ and $\gamma - A'$ self energy diagrams in Figures 2.2, 2.3, 2.4, respectively.

Before going into the details, the dark photon will be introduced.

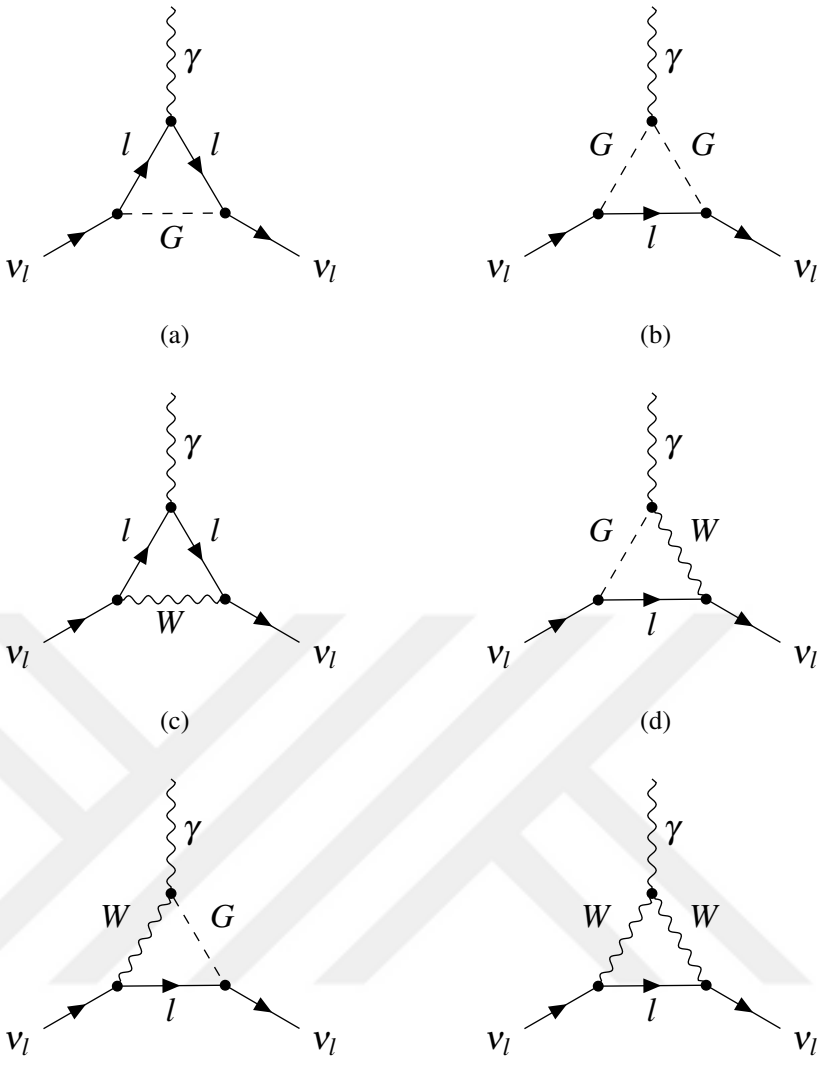

Figure 2.2: Proper vertice diagrams contribute to the electromagnetic vertex function of the neutrino. G is the Goldstone boson and l is the corresponding lepton to the neutrino.

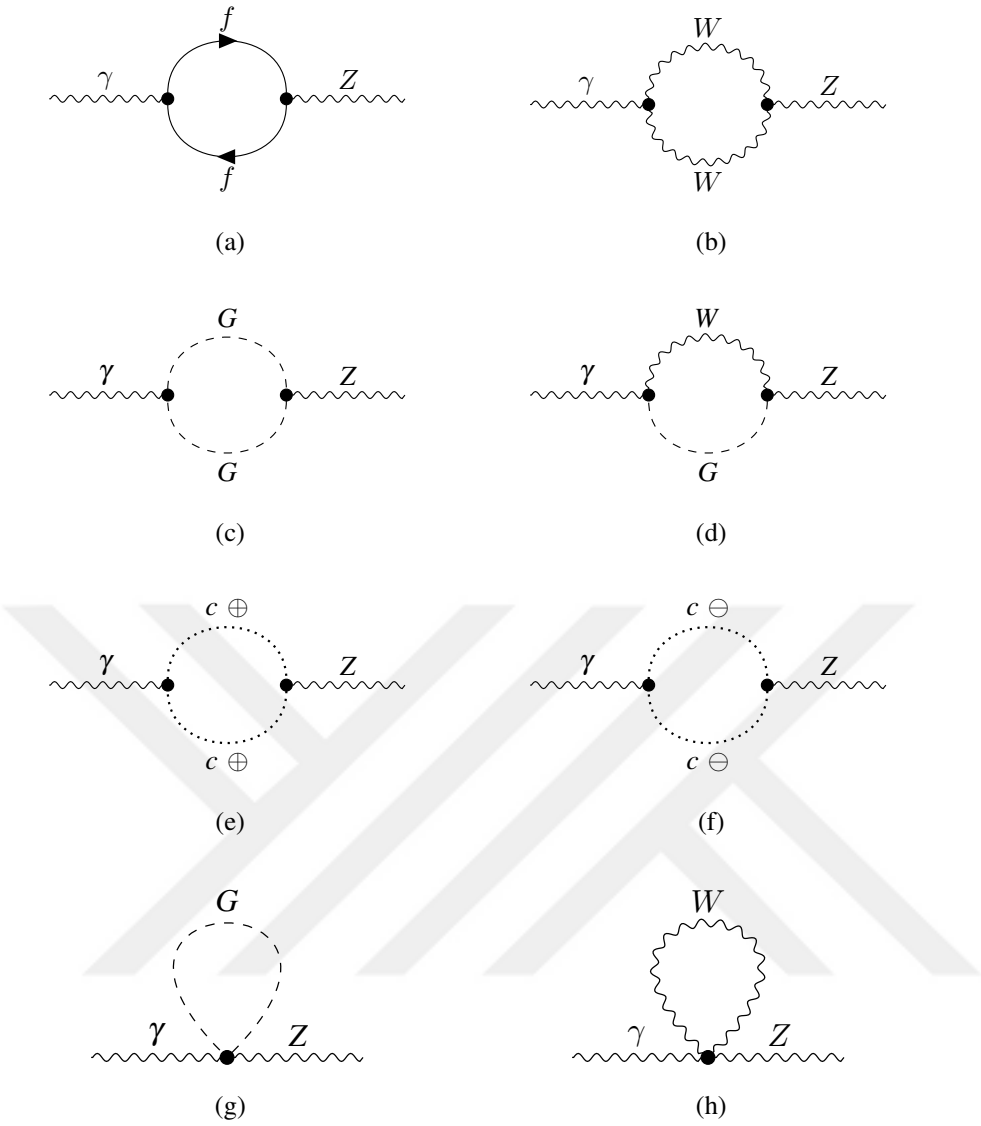

Figure 2.3: The $\gamma - Z$ self-energy diagrams. f denotes the e, μ, and τ lepton as well as $u,\ c,\ t,\ d,\ s$, and b quarks. G is the Goldstone boson, $c \oplus$ and $c \ominus$ are charged Ghosts.

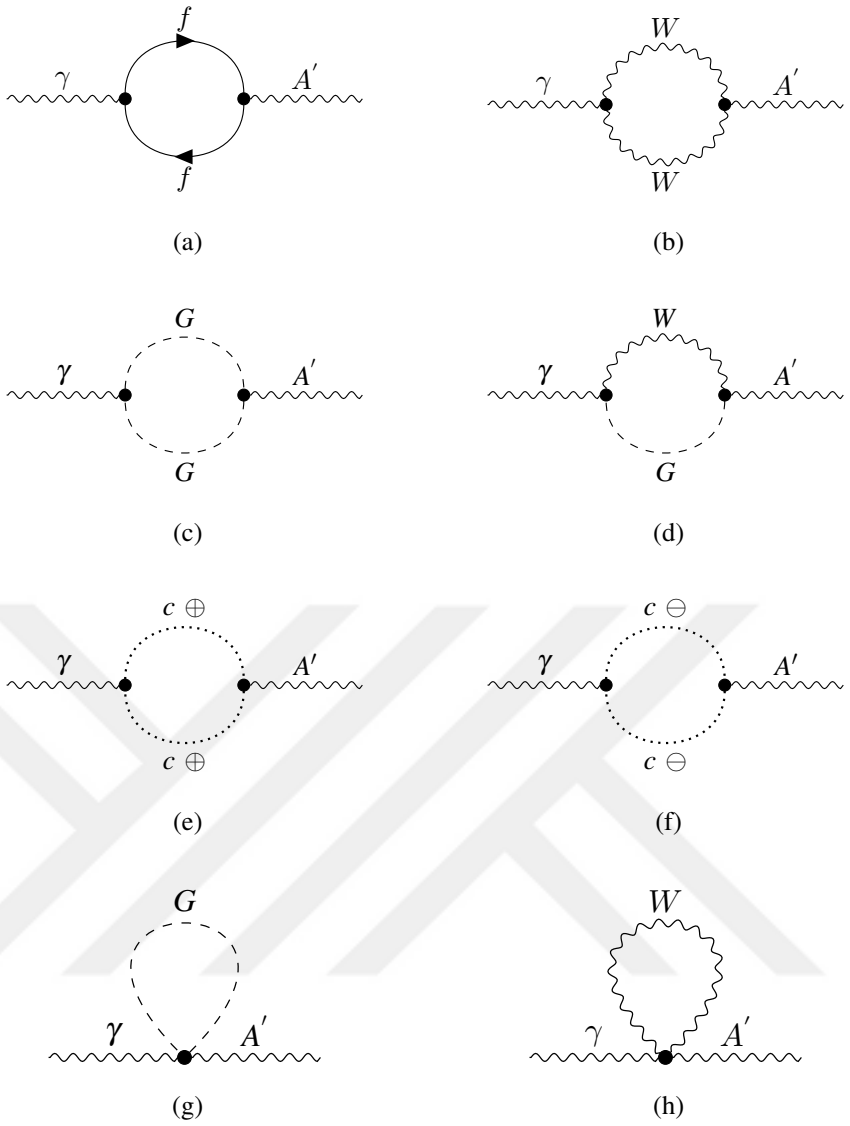

Figure 2.4: The $\gamma - A'$ self-energy diagrams. f denotes the e, μ, and τ lepton as well as $u,\ c,\ t,\ d,\ s$, and b quarks. G is the Goldstone boson, $c \oplus$ and $c \ominus$ are charged Ghosts.

2.2 The Dark Photon

$U_{B-L}(1)$ model is formed by the addition of an abelian symmetry as an extra $U(1)$ to the SM as $SU(2)_L \times U(1)_Y \times U_{B-L}(1)$. The new $U_{B-L}(1)$ field is kinetically mixed with the SM $U(1)_Y$ hypercharge field [63–65]. This kinetic mixing is always possible because the field strengths of two Abelian gauge fields can be multiplied together to give a dimension four operator whose existence means that as the two gauge bosons propagate, they can go into each other. The SM particles with charge $Q_D = (B - L)$, where L is the lepton number and B is the baryon number of the corresponding particle, couple to the new field, which is the dark photon field. The Lagrangian is,

$$\begin{aligned}\mathcal{L} \supset & -\frac{1}{4}W^a_{\mu\nu}W^{a\mu\nu} - \frac{1}{4}B^0_{\mu\nu}B^{0\mu\nu} - \frac{\sin(\epsilon)}{2}B^0_{\mu\nu}X^{0\mu\nu} - \frac{1}{4}X^0_{\mu\nu}X^{0\mu\nu} \\ & + \frac{1}{2}m_{X_0}X^0_\mu X^{0\mu} + \left(D_\mu \langle H\rangle\right)\left(D_\mu \langle H\rangle\right)^\dagger + \bar{f}_i i \not{D} f_i\end{aligned} \tag{2.9}$$

where W^a, B^0, and X^0 are $SU_L(2)$, $U_Y(1)$ and $U_{B-L}(1)$ gauge fields, respectively. H is the Higgs field and f_i are the fermions. In matrix form,

$$\mathcal{L} = \begin{pmatrix} B^0_\mu & W_{3\mu} & X^0_\mu \end{pmatrix} \underbrace{\begin{pmatrix} 1 & 0 & \sin(\epsilon) \\ 0 & 1 & 0 \\ \sin(\epsilon) & 0 & 1 \end{pmatrix}}_{V} \begin{pmatrix} B^0_\mu \\ W_{3\mu} \\ X^0_\mu \end{pmatrix} \tag{2.10}$$

In this Lagrangian, the Z boson and photon fields are not in physical basis. The Z boson and photon fields should be in physical form and the mixing between the two $U(1)$ fields should be removed. Change of basis from $\left(B^0_\mu\, W_{3\mu}\, X^0_\mu\right)$ to $(B_\mu\, W_{3\mu}\, X_\mu)$ will be applied so the kinetic terms in this Lagrangian become canonical and this is done by transforming the matrix V by a transformation R_1 which is of the form,

$$R_1 = \begin{pmatrix} 1 & 0 & \sin(\epsilon) \\ 0 & 1 & 0 \\ 0 & 0 & \cos(\epsilon) \end{pmatrix} \tag{2.11}$$

After this transformation, the kinetic terms in the Lagrangian $\mathcal{L}$ became canonical, however the mass terms have a non-diagonal form. Another transformation is required to obtain a physical basis where gauge bosons are mass eigenstates with canonical kinetic terms. Initially, the mass Lagrangian has a form,

$$\mathcal{L}_{mass} = \frac{1}{4} m_{X_0}^2 X_{\mu\nu}^0 X^{0\mu\nu} + \left(D_\mu \langle H \rangle\right) \left(D_\mu \langle H \rangle\right)^\dagger \tag{2.12}$$

where, $D_\mu = \partial_\mu - ig\vec{t} \cdot \vec{W}_\mu^a - ig^0 Y B_\mu^0 - ig_{BL} Q_D X_\mu^0$.

The vacuum expectation of the Higgs field is $\langle H \rangle = \begin{pmatrix} 0 & \frac{v}{\sqrt{2}} \end{pmatrix}^T$ and quantum numbers are $Q_D^H = 0$, $Y = \frac{1}{2}$, and $t_3 = -\frac{1}{2}$. After the first transformation and change of basis, the Lagrangian becomes,

$$\mathcal{L}_{mass} = \frac{1}{2} m_{X_0} \sec^2(\epsilon) X_{\mu\nu} X^{\mu\nu} + \frac{v^2}{2} \left\{ -g t_3 W_{3\mu} - g' Y B_\mu + g' Y \tan(\epsilon) X_\mu \right\}^2 \tag{2.13}$$

Using the Weinberg mixing angle $\sin(\theta_W) = \frac{g'}{\sqrt{g^2 + g'^2}}$,

$$\begin{aligned} \mathcal{L}_{mass} &= \frac{1}{2} m_{X_0} \sec^2(\epsilon) X_{\mu\nu} X^{\mu\nu} + \frac{v^2}{8} \left(g^2 + g'^2\right) \left\{ g W_{3\mu} - g' B_\mu + g' \tan(\epsilon) X_\mu \right\}^2 \\ &= \frac{1}{2} m_{X_0} \sec^2(\epsilon) X_{\mu\nu} X^{\mu\nu} + \\ &\quad \frac{v^2}{8} \left(g^2 + g'^2\right) \left\{ \cos(\theta_W) W_{3\mu} - \sin(\theta_W) B_\mu + \sin(\theta_W) \tan(\epsilon) X_\mu \right\}^2 \end{aligned} \tag{2.14}$$

Define an intermediate basis $\begin{pmatrix} A_\mu & \hat{W}_{3\mu} & X_\mu \end{pmatrix}$ where $\hat{W}_{3\mu}$ is defined as,

$$\hat{W}_{3\mu} = \cos(\theta_W) W_{3\mu} - \sin(\theta_W) B_\mu \tag{2.15}$$

The photon field A_μ is $A_\mu = \cos\theta_W B_\mu + \sin\theta_W W_{3\mu}$ and remains massless. Then the mass Lagrangian becomes,

$$\begin{aligned}\mathcal{L}_{mass} &= \frac{1}{2}m_{X_0}\sec^2(\epsilon)X_{\mu\nu}X^{\mu\nu} + \frac{1}{2}m_{Z_0}^2\left\{\hat{W}_{3\mu} + \sin(\theta_W)\tan(\epsilon)X_\mu\right\}^2 \\ &= \begin{pmatrix} A_\mu & \hat{W}_{3\mu} & X_\mu \end{pmatrix} M_{\hat{A}}^2 \begin{pmatrix} A_\mu \\ \hat{W}_{3\mu} \\ X_\mu \end{pmatrix}\end{aligned} \tag{2.16}$$

where $m_{Z_0}^2 = \frac{1}{4}\left(g^2 + g'^2\right)v^2$ and $M_{\hat{A}}^2$ is,

$$M_{\hat{A}}^2 = \begin{pmatrix} 0 & 0 & 0 \\ 0 & m_{Z_0}^2 & m_{Z_0}^2\tan(\epsilon)\sin(\theta_W) \\ 0 & m_{Z_0}^2\tan(\epsilon)\sin(\theta_W) & m_{X_0}^2\sec^2(\epsilon) + m_{Z_0}^2\tan^2(\epsilon)\sin^2(\theta_W) \end{pmatrix} \tag{2.17}$$

In this basis, the only the photon field is physical and the mass terms of the $\hat{W}_{3\mu}$ and X_μ is mixed. In order to eliminate the mass mixing between $\hat{W}_{3\mu}$ and X_μ, an orthogonal transformation R_2 will be applied and the basis will be changed from $\hat{A}$ to $A = \begin{pmatrix} A_\mu & Z_\mu & A'_\mu \end{pmatrix}$ which will eventually be the physical basis for all the fields.

$$\begin{pmatrix} A_\mu & Z_\mu & A'_\mu \end{pmatrix} = \underbrace{\begin{pmatrix} 1 & 0 & 0 \\ 0 & \cos(\beta) & \sin(\beta) \\ 0 & -\sin(\beta) & \cos(\beta) \end{pmatrix}}_{R_2} \begin{pmatrix} A_\mu \\ \hat{W}_{3\mu} \\ X_\mu \end{pmatrix} \tag{2.18}$$

After applying the transformations R_1 and R_2 , the parameter β can be found as,

$$\tan(2\beta) = \frac{2\tan(\epsilon)\sin(\theta_W)}{1 - \Delta Z\sec^2(\epsilon) - \tan(\epsilon)\sin(\theta_W)} \tag{2.19}$$

and

$$\begin{aligned}\tan(\beta) = &\frac{\sqrt{\left(\Delta Z\sec^2(\epsilon) + \tan^2(\epsilon)\sin^2(\theta_W) - 1\right)^2 + 4\tan^2(\epsilon)\sin^2(\theta_W)}}{2\tan(\epsilon)\sin(\theta_W)} \\ &+ \frac{\Delta Z\sec^2(\epsilon) + \tan^2(\epsilon)\sin^2(\theta_W) - 1}{2\tan(\epsilon)\sin(\theta_W)}\end{aligned} \tag{2.20}$$

where $\Delta Z = m_{X_0}^2/m_{Z_0}^2$. Finally, the mass Lagrangian becomes,

$$\mathcal{L} = \begin{pmatrix} A_\mu & Z_\mu & A'_\mu \end{pmatrix} \begin{pmatrix} 1 & 0 & 0 \\ 0 & M_Z^2 & 0 \\ 0 & 0 & M_{A'}^2 \end{pmatrix} \begin{pmatrix} A_\mu \\ Z_\mu \\ A'_\mu \end{pmatrix} \tag{2.21}$$

Dark photon and Z boson masses are,

$$\begin{aligned} M_{A'}^2 &= m_{Z_0}^2 \left[\sin(\beta) - \cos(\beta)\sin(\theta_W)\tan(\epsilon)\right]^2 + \frac{m_{X_0}^2 \cos^2(\beta)}{\cos^2(\epsilon)} \\ M_Z^2 &= m_{Z_0}^2 \left[\cos(\beta) + \sin(\beta)\sin(\theta_W)\tan(\epsilon)\right]^2 + \frac{m_{X_0}^2 \sin^2(\beta)}{\cos^2(\epsilon)} \end{aligned} \tag{2.22}$$

The same transformations should be applied to the interaction terms in Lagrangian in Equation 2.9 to obtain the interaction of the SM fermions with the dark photon. The couplings of the Z boson and the dark photon to Standard Model neutrino and quarks has given in Table 2.1. After the addition of the dark model to the SM, the couplings of the Z boson with the SM particles have been modified and can be seen in Table 2.1.

Table 2.1: Couplings of the Z boson and the dark photon to Standard Model neutrino and quarks.

	$C_V^f / C_V^{\prime f}$	$C_A^f / C_A^{\prime f}$
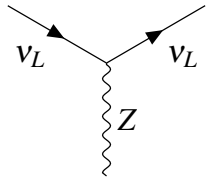	$-\frac{g_{BL}\sin(\beta)}{4\cos(\epsilon)}$ $+\frac{e(\cos(\beta)+\sin(\beta)\tan(\epsilon)\sin(\theta_W))}{4\cos(\theta_W)\sin(\theta_W)}$	$-\frac{g_{BL}\sin(\beta)}{4\cos(\epsilon)}$ $-\frac{e(\cos(\beta)+\sin(\beta)\tan(\epsilon)\sin(\theta_W))}{4\cos(\theta_W)\sin(\theta_W)}$
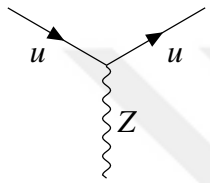	$\frac{g_{BL}\sin(\beta)}{12\cos(\epsilon)}$ $+\frac{e\cos(\beta)(8\sin^2(\theta_W)-3)}{12\cos(\theta_W)\sin(\theta_W)}$ $+\frac{e(5\sin(\beta)\tan(\epsilon)\sin(\theta_W))}{12\cos(\theta_W)\sin(\theta_W)}$	$-\frac{e(\cos(\beta)+\sin(\beta)\tan(\epsilon)\sin(\theta_W))}{4\cos(\theta_W)\sin(\theta_W)}$
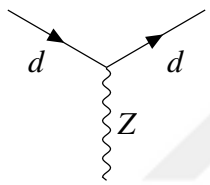	$-\frac{g_{BL}\sin(\beta)}{12\cos(\epsilon)}$ $+\frac{e\cos(\beta)(4\sin^2(\theta_W)-3)}{12\cos(\theta_W)\sin(\theta_W)}$ $+\frac{e\sin(\beta)\tan(\epsilon)\sin(\theta_W)}{12\cos(\theta_W)\sin(\theta_W)}$	$\frac{e(\cos(\beta)+\sin(\beta)\tan(\epsilon)\sin(\theta_W))}{4\cos(\theta_W)\sin(\theta_W)}$
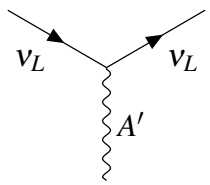	$\frac{g_{BL}\cos(\beta)}{4\cos(\epsilon)}$ $+\frac{e(\sin(\beta)-\cos(\beta)\tan(\epsilon)\sin(\theta_W))}{4\cos(\theta_W)\sin(\theta_W)}$	$\frac{e(\sin(\beta)-\cos(\beta)\tan(\epsilon)\sin(\theta_W))}{4\cos(\theta_W)\sin(\theta_W)}$
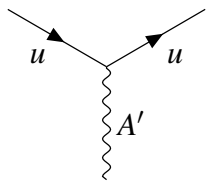	$\frac{g_{BL}\cos(\beta)}{12\cos(\epsilon)}$ $-\frac{e(5\cos(\beta)\tan(\epsilon)\sin(\theta_W))}{12\cos(\theta_W)\sin(\theta_W)}$	$\frac{e(\sin(\beta)-\cos(\beta)\tan(\epsilon)\sin(\theta_W))}{4\cos(\theta_W)\sin(\theta_W)}$
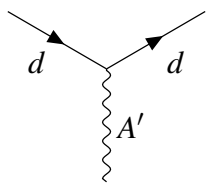	$-\frac{g_{BL}\cos(\beta)}{12\cos(\epsilon)}$ $+\frac{e\sin(\beta)(4\sin^2(\theta_W)-3)}{12\cos(\theta_W)\sin(\theta_W)}$ $-\frac{e\cos(\beta)\tan(\epsilon)\sin(\theta_W)}{12\cos(\theta_W)\sin(\theta_W)}$	$-\frac{e(\sin(\beta)-\cos(\beta)\tan(\epsilon)\sin(\theta_W))}{4\cos(\theta_W)\sin(\theta_W)}$

2.3 Results

2.3.1 Magnetic Moment and Charge Radius of the Neutrino

The magnetic moment of a neutrino has been calculated [66] in the extended Standard Model in which a right handed $SU(2)$ singlet neutrino is introduced. An example calculation will be carried out to understand which diagrams in Figures 2.2,2.3 and 2.4 has a contribution to the magnetic moment of the neutrino. The gauge has chosen as the Feynman gauge. Electromagnetic vertex function of the electron-type neutrino in the diagram in Figure 2.5 is,

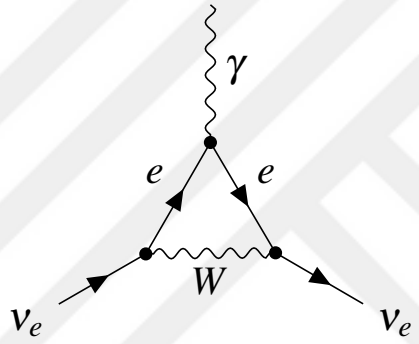

Figure 2.5: A diagram that contributes to the neutrino magnetic moment

$$\Lambda_\mu = \frac{\begin{array}{c} i\mathrm{e}^3 \cdot \gamma^v \cdot \left(\frac{1}{2} - \frac{\bar{\gamma}^5}{2}\right) \cdot (\gamma \cdot (k + p_2) + m_e) \cdot \gamma^\mu \\ (\gamma \cdot (k + p_1) + m_e) \cdot \gamma^\alpha \cdot \left(\frac{1}{2} - \frac{\bar{\gamma}^5}{2}\right) \end{array}}{32\pi^4 \left(\sin\left(\theta_W\right)\right)^2 \left(k^2 - m_W^2\right) \left((k + p_1)^2 - m_e^2\right) \left((k + p_2)^2 - m_e^2\right)} \tag{2.23}$$

where the expressions with a bar represent the objects living in the 4-dimensional space and the rest is in the D-dimensional space. Applying Dirac equation and using the properties and relations of the Dirac matrices, neutrino vertex function is calculated. The term that defines the magnetic moment of the neutrino is,

$$
\begin{aligned}
\Lambda_\mu \supset & \frac{1}{32\pi^2\left(\sin\left(\theta_W\right)\right)^2} i\mathrm{e}^3 m_{\nu_e} \cdot \left(p_2^\mu + p_1^\mu\right) \\
& \Big[2\mathrm{C}_0\left(m_{\nu_e}^2, m_{\nu_e}^2, 0, m_e^2, m_W^2, m_e^2\right) + D\mathrm{C}_1\left(m_{\nu_e}^2, 0, m_{\nu_e}^2, m_W^2, m_e^2, m_e^2\right) \\
& + 2\mathrm{C}_1\left(m_{\nu_e}^2, 0, m_{\nu_e}^2, m_W^2, m_e^2, m_e^2\right) + D\mathrm{C}_{11}\left(m_{\nu_e}^2, 0, m_{\nu_e}^2, m_W^2, m_e^2, m_e^2\right) \\
& - 2\mathrm{C}_{11}\left(m_{\nu_e}^2, 0, m_{\nu_e}^2, m_W^2, m_e^2, m_e^2\right) \\
& + D\mathrm{C}_{12}\left(m_{\nu_e}^2, 0, m_{\nu_e}^2, m_W^2, m_e^2, m_e^2\right) \\
& - 2\mathrm{C}_{12}\left(m_{\nu_e}^2, 0, m_{\nu_e}^2, m_W^2, m_e^2, m_e^2\right) \Big]
\end{aligned}
\tag{2.24}
$$

where C_0, C_1, C_{11}, C_{12} is the Passarino-Veltman integral representing the loop integrals. The Gordon identity in Equation 2.25 is used to obtain the structure of the magnetic moment form factor in Equation 2.2,

$$
\bar{\varphi}\left(p_2\right)\gamma^\mu\varphi(p_1) = \bar{\varphi}\left(p_2\right)\left[\frac{p_2^\mu + p_1^\mu}{2m} + \frac{i\sigma^{\mu\nu}q_\nu}{2m}\right]\varphi(p_1) \tag{2.25}
$$

putting the Equation 2.25 into the 2.26, the magnetic moment form factor is found to be,

$$
\begin{aligned}
f_M\left(q^2\right) = & \frac{1}{32\pi^2\left(\sin\left(\theta_W\right)\right)^2} i\mathrm{e}^3 m_{\nu_e} \Big[2\mathrm{C}_0\left(m_{\nu_e}^2, m_{\nu_e}^2, 0, m_e^2, m_W^2, m_e^2\right) \\
& + D\mathrm{C}_1\left(m_{\nu_e}^2, 0, m_{\nu_e}^2, m_W^2, m_e^2, m_e^2\right) \\
& + 2\mathrm{C}_1\left(m_{\nu_e}^2, 0, m_{\nu_e}^2, m_W^2, m_e^2, m_e^2\right) \\
& + D\mathrm{C}_{11}\left(m_{\nu_e}^2, 0, m_{\nu_e}^2, m_W^2, m_e^2, m_e^2\right) \\
& - 2\mathrm{C}_{11}\left(m_{\nu_e}^2, 0, m_{\nu_e}^2, m_W^2, m_e^2, m_e^2\right) \\
& + D\mathrm{C}_{12}\left(m_{\nu_e}^2, 0, m_{\nu_e}^2, m_W^2, m_e^2, m_e^2\right) \\
& - 2\mathrm{C}_{12}\left(m_{\nu_e}^2, 0, m_{\nu_e}^2, m_W^2, m_e^2, m_e^2\right) \Big]
\end{aligned}
\tag{2.26}
$$

This result is the contribution of the diagram in Figure 2.5 to the magnetic form factor of the neutrino. However, after calculating all of the diagrams, the ones that contribute to the magnetic moment of the neutrino are only the proper vertices given in Figure 2.2. From the interaction of the dark photon with the neutrino and other visible matter

in the model described above, there is no contribution from the dark photon to the proper vertex diagrams. Therefore, it is concluded that the dark photon does not contribute to the magnetic dipole form factor. On the other hand, all diagrams have contributions for the electric form factor since γ_μ structure exists in every diagram included. Neutrino vertex function in Equation 2.23 contains the term,

$$\begin{aligned}
\Lambda_\mu \supset -\frac{1}{64\pi^2 \sin^2(\theta_W)}\, \mathrm{e}^3 \gamma^\mu \Big[& D\, \mathrm{B}_0\left(0, m_e^2, m_e^2\right) + 4\, \mathrm{B}_0\left(m_{\nu_e}^2, m_e^2, m_W^2\right) \\
& - 6\, \mathrm{B}_0\left(0, m_e^2, m_e^2\right) - D m_e^2 \mathrm{C}_0\left(m_{\nu_e}^2, m_{\nu_e}^2, 0, m_e^2, m_W^2, m_e^2\right) \\
& + D m_W^2 \mathrm{C}_0\left(m_{\nu_e}^2, m_{\nu_e}^2, 0, m_e^2, m_W^2, m_e^2\right) \\
& - D m_{\nu_e}^2 \mathrm{C}_0\left(m_{\nu_e}^2, m_{\nu_e}^2, 0, m_e^2, m_W^2, m_e^2\right) \\
& + 6 m_e^2 \mathrm{C}_0\left(m_{\nu_e}^2, m_{\nu_e}^2, 0, m_e^2, m_W^2, m_e^2\right) \\
& - 6 m_W^2 \mathrm{C}_0\left(m_{\nu_e}^2, m_{\nu_e}^2, 0, m_e^2, m_W^2, m_e^2\right) \\
& + 6 m_{\nu_e}^2 \mathrm{C}_0\left(m_{\nu_e}^2, m_{\nu_e}^2, 0, m_e^2, m_W^2, m_e^2\right) \\
& - 2D \mathrm{C}_{00}\left(m_{\nu_e}^2, 0, m_{\nu_e}^2, m_W^2, m_e^2, m_e^2\right) \\
& + 4 \mathrm{C}_{00}\left(m_{\nu_e}^2, 0, m_{\nu_e}^2, m_W^2, m_e^2, m_e^2\right) \Big]
\end{aligned} \tag{2.27}$$

and this is the electric form factor in the Equation 2.2. The neutrino charge radius can be found using the Equation 2.8.

After calculating the matrix elements of all of the diagrams in Figure 2.2, Figure 2.3, and Figure 2.4, the charge radius of the neutrino in the one-loop limit in the $U_{B-L}(1)$ model is calculated. From the diagrams, couple of them are calculated manually to understand the structure and the terms that arise from each type of diagram. Calculation of the vertex functions and one-loop integrals are handled with the help of publically available Mathematica packages, FeynCalc [67, 68] and FeynArts [69]. Then, after the one-loop integrals are converted into the Passarino-Veltman functions, their explicit forms are obtained by taking the integrals with the help of the PackageX [70]. The diagrams a,b,c and f in Figure 2.2; b, c, d, e, f, g, and h given in Figure 2.3 and Figure 2.4 contain ultraviolet divergent terms given in Tables 2.2, 2.3, and 2.4 and their summation is found to be zero. The expression of the charge radius is,

$$
\begin{aligned}
\left\langle r^2 \right\rangle = & \frac{6}{2\pi^2 v^3 M_{A'}^4 M_Z^4 \cos(\epsilon)\cos^2(\theta_W)} \ln(2\pi) m_W^4 \sin(\theta_W) \\
& \Big\{ 2 m_W \cos(\epsilon)\cos^2(\theta_W)\sin(\theta_W)\big[\sin(\theta_W)\left(\cos^2(\beta) M_{A'}^4 + M_Z^4 \sin^2(\beta)\right) \\
& + \cos(\beta)\sin(\beta)\tan(\epsilon)\left(M_{A'}^4 - M_Z^4\right)\big] \\
& + m_W \cos(\epsilon)\cos^4(\theta_W)\left(\cos^2(\beta) M_{A'}^4 + M_Z^4 \sin^2(\beta)\right) \\
& + m_W \cos(\epsilon)\sin^2(\theta_W)\big[\sin^2(\theta_W)\left(\cos^2(\beta) M_{A'}^4 + M_Z^4 \sin^2(\beta)\right) \\
& + \tan^2(\epsilon)\left(\cos^2(\beta) M_Z^4 + M_{A'}^4 \sin^2(\beta)\right) \\
& + 2\cos(\beta)\sin(\beta)\tan(\epsilon)\left(M_{A'}^4 - M_Z^4\right)\sin(\theta_W)\big] \\
& - 2 v g_{BL} \cos(\theta_W)\sin(\theta_W)\big[\tan(\epsilon)\left(\cos^2(\beta) M_Z^4 + M_{A'}^4 \sin^2(\beta)\right) \\
& + \cos(\beta)\sin(\beta)\left(M_{A'}^4 - M_Z^4\right)\sin(\theta_W)\big] \\
& + 2 v g_{BL} \cos(\beta)\sin(\beta)\left(M_Z^4 - M_{A'}^4\right)\cos^3(\theta_W) \Big\}
\end{aligned}
\tag{2.28}
$$

Analytical result obtained for the neutrino charge radius can be used to bound parameter space of the $U_{B-L}(1)$ model. The data from scattering experiments such as neutrino-electron scattering and coherent elastic neutrino nucleus scattering CEνNS can be used for this purpose since the diagrams of the charge radius also contribute to the scattering processes mentioned above which are expected to be sensitive to the light dark photon region.

Table 2.2: Divergent parts of the proper vertex diagrams given in Figure 2.2 corresponding to the process $\nu_e \to \gamma\nu_e$ in Section 2.3.1

Proper Vertex Diagrams	
Diagram Label	Divergent part
a	$-\dfrac{m_e^2 m_W \sin(\theta_W)}{16\pi^2 v^3}$
b	$\dfrac{m_e^2 m_W \sin(\theta_W)}{16\pi^2 v^3}$
c	$-\dfrac{m_W^3 \sin(\theta_W)}{8\pi^2 v^3}$
f	$\dfrac{3m_W^3 \sin(\theta_W)}{8\pi^2 v^3}$

Table 2.3: Divergent parts of the self-energy diagrams given in Figure 2.3 corresponding to the process $\nu_e \to \gamma\nu_e$ in Section 2.3.1

$\gamma - Z$ Self-Energy Diagrams	
Diagram Label	Divergent part
b	$-\frac{9}{8\pi^2 v^3 \cos(\epsilon) m_Z^2}\cos(\beta) m_W^4 \sin(\theta_W)$ $\big[\cos(\beta)\cos(\epsilon) m_W \cos^2(\theta_W) + \cos(\epsilon) m_W \sin(\theta_W)\big(\cos(\beta)\sin(\theta_W)$ $+ \sin(\beta)\tan(\epsilon)\big) - 2 g_{BL}\sin(\beta) v \cos(\theta_W)\big]$
c	$\frac{1}{8\pi^2 v^3 \cos(\epsilon) m_Z^2 \cos^2(\theta_W)} m_W^4 \sin(\theta_W)$ $\big[-\cos^2(\beta)\cos(\epsilon) m_W \cos^4(\theta_W) - 2 v g_{BL}\cos(\theta_W)\sin(\theta_W)$ $\times\big(-\cos^2(\beta)\tan(\epsilon) + \cos(\beta)\sin(\beta)\sin(\theta_W) + \tan(\epsilon)\big)$ $+ \cos(\epsilon) m_W \sin^2(\theta_W)\left(\cos(\beta)\sin(\theta_W) + \sin(\beta)\tan(\epsilon)\right)^2$ $+ 2 v \cos(\beta) g_{BL}\sin(\beta)\cos^3(\theta_W)\big]$
d_1	$-\frac{1}{8\pi^2 v^3 \cos(\epsilon) m_Z^2 \cos^2(\theta_W)} m_W^4 \sin^2(\theta_W)$ $\left(\cos(\beta)\sin(\theta_W) + \sin(\beta)\tan(\epsilon)\right)\big[\cos(\beta)\cos(\epsilon) m_W \cos^2(\theta_W)$ $+ \cos(\epsilon) m_W \sin(\theta_W)\big(\cos(\beta)\sin(\theta_W)$ $+ \sin(\beta)\tan(\epsilon)\big) - 2 g_{BL}\sin(\beta) v \cos(\theta_W)\big]$
d_2	$-\frac{1}{8\pi^2 v^3 \cos(\epsilon) m_Z^2 \cos^2(\theta_W)}$ $m_W^4 \sin^2(\theta_W)\left(\cos(\beta)\sin(\theta_W) + \sin(\beta)\tan(\epsilon)\right)$ $\big[m_W \cos(\beta)\cos(\epsilon)\cos^2(\theta_W) + m_W \cos(\epsilon)\sin(\theta_W)\big(\cos(\beta)\sin(\theta_W)$ $+ \sin(\beta)\tan(\epsilon)\big) - 2 v g_{BL}\sin(\beta)\cos(\theta_W)\big]$

Table 2.4: Divergent parts of the self-energy diagrams given in Figure 2.3 corresponding to the process $\nu_e \to \gamma\nu_e$ in Section 2.3.1

$\gamma - Z$ Self-Energy Diagrams	
Diagram Label	Divergent part
e	$\frac{1}{16\pi^2 v^3 \cos(\epsilon) m_Z^2} m_W^4 \cos(\beta)\sin(\theta_W)$ $\big[\cos(\beta)\cos(\epsilon) m_W \cos^2(\theta_W)$ $+ m_W \cos(\epsilon)\sin(\theta_W)\left(\cos(\beta)\sin(\theta_W) + \sin(\beta)\tan(\epsilon)\right)$ $- 2 g_{BL}\sin(\beta) v \cos(\theta_W)\big]$
f	$\frac{1}{16\pi^2 \cos(\epsilon) v^3 m_Z^2} \cos(\beta) m_W^4 \sin(\theta_W)$ $\big[\cos(\beta)\cos(\epsilon) m_W \cos^2(\theta_W)$ $+ \cos(\epsilon) m_W \sin(\theta_W)\left(\cos(\beta)\sin(\theta_W) + \sin(\beta)\tan(\epsilon)\right)$ $- 2 g_{BL}\sin(\beta) v \cos(\theta_W)\big]$
g	$-\frac{1}{8\pi^2 v^3 \cos(\epsilon) m_Z^2 \cos^2(\theta_W)} m_W^4 \sin(\theta_W)$ $\big[- m_W \cos^2(\beta)\cos(\epsilon)\cos^4(\theta_W)$ $- 2 v g_{BL}\cos(\theta_W)\sin(\theta_W)\big(- \cos^2(\beta)\tan(\epsilon) + \tan(\epsilon)$ $+ \cos(\beta)\sin(\beta)\sin(\theta_W)\big)$ $+ \cos(\epsilon) m_W \sin^2(\theta_W)\left(\cos(\beta)\sin(\theta_W) + \sin(\beta)\tan(\epsilon)\right)^2$ $+ 2 v g_{BL}\cos(\beta)\sin(\beta)\cos^3(\theta_W)\big]$
h	$\frac{3}{4\pi^2 v^3 \cos(\epsilon) m_Z^2} \cos(\beta) m_W^4 \sin(\theta_W)$ $\big[\cos(\beta)\cos(\epsilon) m_W \cos^2(\theta_W)$ $+ \cos(\epsilon) m_W \sin(\theta_W)\left(\cos(\beta)\sin(\theta_W) + \sin(\beta)\tan(\epsilon)\right)$ $- 2 v g_{BL}\sin(\beta)\cos(\theta_W)\big]$

Table 2.5: Divergent parts of the self-energy diagrams in Figure 2.4 corresponding to the process $\nu_e \to \gamma\nu_e$ in Section 2.3.1

$\gamma - A'$ Self-Energy Diagrams	
Diagram Label	Divergent part
b	$-\frac{9}{8\pi^2 v^3 \cos(\epsilon) M_{A'}^2} m_W^4 \sin(\beta)\sin(\theta_W)$ $\big[m_W \cos(\epsilon)\sin(\theta_W)\big(\sin(\beta)\sin(\theta_W) - \cos(\beta)\tan(\epsilon)\big)$ $+ 2v g_{BL}\cos(\beta)\cos(\theta_W) + m_W \cos(\epsilon)\sin(\beta)\cos^2(\theta_W)\big]$
c	$-\frac{1}{8\pi^2 v^3 \cos^2(\theta_W)\cos(\epsilon) M_{A'}^2} m_W^4 \sin(\theta_W)$ $\big[\sin(\theta_W)\left(\cos(\beta)\tan(\epsilon) - \sin(\beta)\sin(\theta_W)\right) + \sin(\beta)\cos^2(\theta_W)\big]$ $\big[m_W \cos(\epsilon)\sin(\theta_W)\left(\sin(\beta)\sin(\theta_W) - \cos(\beta)\tan(\epsilon)\right)$ $+ 2v g_{BL}\cos(\beta)\cos(\theta_W) + \cos(\epsilon)\sin(\beta) m_W \cos^2(\theta_W)\big]$
d_1	$\frac{1}{8\pi^2 v^3 \cos^2(\theta_W)\cos(\epsilon) M_{A'}^2} m_W^4 \sin^2(\theta_W)$ $\big[\cos(\beta)\tan(\epsilon) - \sin(\beta)\sin(\theta_W)\big]$ $\big[m_W \cos(\epsilon)\sin(\theta_W)\big(\sin(\beta)\sin(\theta_W) - \cos(\beta)\tan(\epsilon)\big)$ $+ 2v g_{BL}\cos(\beta)\cos(\theta_W) + \cos(\epsilon)\sin(\beta) m_W \cos^2(\theta_W)\big]$
d_2	$\frac{1}{8\pi^2 v^3 \cos^2(\theta_W)\cos(\epsilon) M_{A'}^2} m_W^4 \sin^2(\theta_W)$ $\big[\cos(\beta)\tan(\epsilon) - \sin(\beta)\sin(\theta_W)\big]$ $\big[m_W \cos(\epsilon)\sin(\theta_W)\left(\sin(\beta)\sin(\theta_W) - \cos(\beta)\tan(\epsilon)\right)$ $+ 2v g_{BL}\cos(\beta)\cos(\theta_W) + m_W \cos(\epsilon)\sin(\beta)\cos^2(\theta_W)\big]$

Table 2.6: Divergent parts of the self-energy diagrams in Figure 2.4 corresponding to the process $\nu_e \to \gamma\nu_e$ in Section 2.3.1

$\gamma - A'$ Self-Energy Diagrams	
Diagram Label	Divergent part
e	$\frac{1}{16\pi^2 v^3 \cos(\epsilon) M_{A'}^2} m_W^4 \sin(\beta)\sin(\theta_W)$ $\big[\cos(\epsilon) m_W \sin(\theta_W)\,(\sin(\beta)\sin(\theta_W) - \cos(\beta)\tan(\epsilon))$ $+ 2v g_{BL}\cos(\beta)\cos(\theta_W) + \cos(\epsilon)\sin(\beta) m_W \cos^2(\theta_W)\big]$
f	$\frac{1}{16\pi^2 v^3 \cos(\epsilon) M_{A'}^2} m_W^4 \sin(\beta)\sin(\theta_W)$ $\big[\cos(\epsilon) m_W \sin(\theta_W)\,(\sin(\beta)\sin(\theta_W) - \cos(\beta)\tan(\epsilon))$ $+ 2\cos(\beta) g_{BL} v \cos(\theta_W) + \cos(\epsilon)\sin(\beta) m_W \cos^2(\theta_W)\big]$
g	$\frac{1}{8\pi^2 v^3 M_{A'}^2 \cos(\epsilon)\cos^2(\theta_W)} m_W^4 \sin(\theta_W)\big[\sin(\theta_W)\big(\cos(\beta)\tan(\epsilon)$ $- \sin(\beta)\sin(\theta_W)\big) + \sin(\beta)\cos^2(\theta_W)\big]$ $\big[\cos(\epsilon) m_W \sin(\theta_W)\,(\sin(\beta)\sin(\theta_W) - \cos(\beta)\tan(\epsilon))$ $+ 2\cos(\beta) g_{BL} v \cos(\theta_W) + \cos(\epsilon)\sin(\beta) m_W \cos^2(\theta_W)\big]$
h	$\frac{3}{4\pi^2 v^3 \cos(\epsilon) M_{A'}^2} m_W^4 \sin(\beta)\sin(\theta_W)$ $\big[m_W \cos(\epsilon)\sin(\theta_W)\,(\sin(\beta)\sin(\theta_W) - \cos(\beta)\tan(\epsilon))$ $+ 2v g_{BL}\cos(\beta)\cos(\theta_W) + m_W \cos(\epsilon)\sin(\beta)\cos^2(\theta_W)\big]$

CHAPTER 3

PARAMETER SPACE OF FAT-BRANE UNIVERSAL EXTRA DIMENSION MODEL AFTER ATLAS MULTI-JET AND PHOTON PLUS JET SEARCHES AT 13 TEV LHC DATA

3.1 Universal Extra Dimensions (UED) and Minimal Universal Extra Dimensions (mUED) Models

The Universal Extra Dimensions (UED) is a general name given to particle physics models created by compactifying m extra dimensions, in size of the order of TeV^{-1}, on different geometries and preserving the gauge symmetry of the SM and then moving them into $3+1+m$ dimensional space. In UED models, all fundamental particles in the SM are assumed to be able to reach small extra dimensions, and due to compactification, the existence of a Kaluza-Kelin (KK) particle tower is expected. Each level in the KK tower is identified by the integer (KK-number). Due to the conservation of translational symmetry in the extra dimensions, the KK-number is conserved in interactions with KK particles. On the other hand, adding Z_2 symmetry to the model is necessary to preserve the SM's chiral structure that is seen in $3+1$ dimensional space-time and eliminate unwanted particle modes. For example, in the constrained variant of the model (minimal UED (mUED)), there is one extra spatial dimension compactified on the semicircle of $\frac{S_1}{Z_2}$, and due to the Z_2 symmetry added to the model, translational symmetry of the extra dimension has been broken. As a result, the KK-number is broken at the first mode level and KK-parity ($\equiv (-1)^n$) symmetry remains. This finite symmetry has several interesting consequences. First, level-1 KK particles can only be produced in pairs in collider experiments as a result of this symmetry. Also, contributions of KK particles to electroweak (EW) parameters are possible only at the mode levels. Another significant result of KK-parity

is that it allows the relatively heavy level-1 KK particles in the spectrum to decay into lighter level-1 particles while keeping the lightest KK (LKP) particle stable and presents a cosmologically suitable cold dark matter candidate. Level-1 KK gluons and quarks (doublet, singlet) have colour charges, and they can be produced in pairs in collider experiments with higher cross sections compared to electroweak gauge bosons. As one can see in the literature, multi-jet, multi-lepton and missing transverse energy signals [71–75] are expected due to the sequential decay of the aforementioned particles. This signal type is similar to SUSY models with the degenerate mass spectrum and conserved R-parity [76], and KK particles have higher cross-section values compared to SUSY particles due to their spin values at similar mass order [77, 78].

The mUED model draws attention as it is the minimum model among the UED model frameworks. In the model, there is only one extra dimension with the size of $\sim \mathcal{O}(\text{TeV}^{-1})$. As a result of the extra dimension compactified on the $\frac{S_1}{Z_2}$ semicircle, there is an expected mass at every $n > 0$ level. The mass of the level-n KK particle is roughly $m_n^2 = m_0^2 + (nR^{-1})^2$ where m_0 represents the SM mass corresponding to the particle and R represents the radius of the extra dimension. Even with relatively small values of $R^{-1} \geq 500GeV$, mUED expects a highly degenerate [38] particle spectrum for KK particles, and thus the decay channels of the particles are closed. However, by including radiative corrections [18] in the calculations, this degeneration can be partially eliminated, and the decay of high-mass particles can be possible. Since the model is higher-dimensional and non-renormalizable, it is assumed that it is valid only up to the energy level $\Lambda \gtrsim R^{-1}$, and beyond this level, other dynamics will arise and renormalize the model. As such, the particle mass spectrum of the model can be clarified with only two parameters (Λ,R); thus, radiative corrections will determine the collider phenomenology of the model. In addition to the radiative corrections expected from the 4-dimensional Minkowskian space-time to the masses of the particles in the model, due to a new extra dimension compacted on the semicircle, two new types of corrections occur: (i) bulk corrections, (ii) boundary corrections. Bulk corrections exist only for KK excitations of gauge bosons and are finite corrections resulting from compactified extra-dimensional turns of internal nodes. Boundary corrections are due to the boundary kinetic terms of the particles. The corrections for these terms, which are assumed to disappear in the model's upper validity limit Λ,

are divergent and directly proportional to $\ln\left(\frac{\Lambda^2}{\mu^2}\right)$. In the expression, μ represents the renormalization scale. Λ is the main parameter in determining the masses of particles in the mUED model since the bulk corrections are smaller than the boundary corrections. The condition that the coupling of the $U\left(1\right)$ gauge symmetry remains perturbative gives the upper limit value $\Lambda \leq 40\ R^{-1}$. The radiative corrections specific to the mUED model can be accessed from [18].

In the model, by diagonalizing the following mass squared matrix, the mixing of excited KK uncharged electro-weak gauge bosons is similar to that in SM, with eigenvalues (masses) and eigenstates of KK-photon and KK-Z bosons are determined,

$$\begin{pmatrix} \frac{\mathrm{n}^2}{\mathrm{R}^2} + \hat{\delta}\mathrm{m}^2_{\mathrm{B^n}} + \frac{1}{4}\,\mathrm{g}^2\mathrm{v}^2 & \frac{1}{4}\mathrm{g}\mathrm{g}'\mathrm{v}^2 \\ \frac{1}{4}\mathrm{g}\mathrm{g}'\mathrm{v}^2 & \frac{\mathrm{n}^2}{\mathrm{R}^2} + \hat{\delta}\mathrm{m}^2_{\mathrm{W^n}} + \frac{1}{4}\,\mathrm{g}'^2\mathrm{v}^2 \end{pmatrix} \tag{3.1}$$

In Equation 3.1 , $\hat{\delta}m^2_{B^n}$ and $\hat{\delta}m^2_{W^n}$, $B^{(n)}_\mu$ and $W^{3(n)}_\mu$ are corrections the first mode level for the gauge bosons, g' and g represent gauge couplings of $U\left(1\right)$ and $SU\left(2\right)_L$ respectively. Another important consequence of the mixing matrix above is that even at reasonable values such as $R^{-1} \geq 500\ GeV$, the mixing of high-level KK particles remains at low levels. Thus, for most of the mUED parameter space, the physical particles Z^1 and γ^1 are basically $W^1_{3\mu}$ and B^1_μ and that leads to significant effects on the signals of particles from collider experiments.

The model considered within the scope of this thesis is a variant of the mUED model, briefly fat-brane UED [79–86] model. The fat-brane model is the model obtained by embedding the space-time structure in the mUED on the 4+N dimensional bulk, under the assumption of N large extra dimensions, in the range of $\sim eV^{-1}$ to keV^{-1}, that only gravity can reach. The fat-brane model consists of the small single extra dimension (accessible to both gravity and the SM) that can be realised as the thickness of the SM three-brane in the $(4+N)$-dimensional bulk, all of which only gravity can access. Thus, in the fat-brane model, both the SM particles and the graviton have KK excitations at different masses due to different compactification orders (eV^{-1} and TeV^{-1}). A unique feature of the model compared to mUED is that neither the KK-number nor the KK-parity is conserved under gravity-mediated decays (GMD). For example, due to GMD, direct decays of level-1 KK particles into lighter SM

particles and graviton, which is not possible in mUED (or, more generally, UED models), are allowed, and the stability of LKP is lost. In this context, the expected signals of fat-brane models in collider experiments may differ drastically from that of mUED [87, 88].

In the model, what makes the collider experiments even more interesting is the cases where gravity-mediated decays occur at a higher rate than KK-number conserved decays (KKCD). In this case, the produced level-1 KK gluons and/or quarks decay directly into the SM particle and graviton and form the di-jet and the signal of missing transverse energy originating from invisible graviton in the detector. Studies examining the model with this perspective are available in the literature [87]. Other signals that can be expected from the model occur when KKCD is higher than or equal to GMD. In the case where KKCD is higher, for example, the level-1 KK particles produced as a result of the collision decay into level-1 KK and SM particles with lower masses by successive decays. $\gamma\gamma$ / γZ / ZZ and the missing transverse energy signals can be observed at the detector.

The last case is when KKCD and GMD are comparable to each other. In this case, for example, one of the pair generated massive level-1 particles decays sequentially over KKCD and eventually produces γZ-boson and graviton, while the other undergoes GMD-type decay and decays directly into graviton and SM particle and can form γZ and the missing transverse energy signal in the detector. In the literature, the parameters of the model were constrained by the $\gamma\gamma$ final signal [87, 88], and another signal type, γj and missing transverse energy final signal, which can be expected from the model and has not been examined before, is examined in this thesis.

3.1.1 Fat-Brane UED Model and Interaction of Gravitation with Matter

3.1.1.1 Kaluza-Klein Tower

With the addition of one extra spatial dimension y to the usual 4-dimensions (4D), one can write the momentum of a particle as

$$E = \sqrt{\vec{p}^2 + p_y^2 + m^2} \equiv \sqrt{\vec{p}^2 + m_{\mathrm{KK}}^2} \tag{3.2}$$

where p_y is the momentum of the particle in the extra dimension and disguise as a mass in the usual 4D space. In the case that the extra dimension extends to infinity, p_y is continuous. However, if the extra spatial dimension is compactified on the circle of radius R, the spectrum of p_y is discrete and number of levels are infinite. As a result, there is a collection of particles with various masses known as the Kaluza-Klein tower (KK-tower).

The metric for the background vacuum can be expressed as,

$$\begin{aligned} ds^2 &= g_{\mathrm{MN}} dX^M dX^N = g_{\mu\nu} dx^\mu dx^\nu - dy^2 \\ g_{\mathrm{MN}} &= \mathrm{diag}(1, -1, -1, -1, -1) \end{aligned} \tag{3.3}$$

where X^M is the 5-dimensional (5D) coordinates and y is assumed to be confined in a circle of $0 \leq y \leq 2\pi R$ so that any function $\phi(x, y)$ is periodic, i.e. $\phi(x, y + 2\pi R) = \phi(x, y)$.

Starting with the action of a massless scalar field in 5D,

$$\begin{aligned} \mathcal{S}^{(5D)} &= \int d^5x \left(\frac{1}{2} \partial_M \Phi(x) \partial^M \Phi(x) \right) \\ &= \int d^4x \int_0^{2\pi R} dy \frac{1}{2} \left[\partial_\mu \Phi(x, \gamma) \partial^\mu \Phi(x, y) - \partial_\gamma \Phi(x, y) \partial_\gamma \Phi(x, \gamma) \right] \end{aligned} \tag{3.4}$$

Periodicity of the y coordinates allows the Fourier expansion of the field,

$$\begin{aligned} \Phi(x, y) &= \frac{1}{\sqrt{2\pi R}} \sum_{n=-\infty}^{+\infty} \varphi^{(n)}(x) e^{\frac{iny}{R}} \\ &= \frac{1}{\sqrt{2\pi R}} \phi^{(0)}(x) + \frac{1}{\sqrt{\pi R}} \sum_{n=1}^{\infty} \left\{ \phi^{(+n)}(x) \cos\left(\frac{ny}{R}\right) + \phi^{(-n)}(x) \sin\left(\frac{ny}{R}\right) \right\} \end{aligned} \tag{3.5}$$

where real scalar fields have been introduced since the scalar field Φ is real, and this implies $\phi^{(-n)} = \phi^{(n)\dagger}$ and

$$\phi^{(-n)} = \phi^{(n)\dagger}, \quad \varphi^{(0)} = \phi^{(0)}, \quad \varphi^{(\pm n)}(n > 0) = \frac{1}{\sqrt{2}}\left(\phi^{(+n)} \mp i\phi^{(-n)}\right) \tag{3.6}$$

Substitute Equation 3.5 into 3.4 and integrate over y,

$$\begin{aligned}\mathcal{S}^{(4D)} &= \int d^4x \, \frac{1}{2}\left[\sum_n \left\{\partial_\mu \varphi^{(-n)} \partial^\mu \varphi^{(n)} - \frac{n^2}{R^2}\varphi^{(-n)}\varphi^{(n)}\right\}\right] \\ &= \int d^4x \, \frac{1}{2}\left[\partial_\mu \phi^{(0)} \partial^\mu \phi^{(0)} + \sum_{n=1}^{\infty}\left\{\partial_\mu \phi^{(\pm n)} \partial^\mu \phi^{(\pm n)} - \frac{n^2}{R^2}\phi^{(\pm n)}\phi^{(\pm n)}\right\}\right]\end{aligned} \tag{3.7}$$

This equation is the 4D effective action that characterizes the field theory in the compactified extra dimensional space. The first term is the typical massless scalar field. By switching to 5D, the second term appears along with an infinite series of massive particles (KK towers) with masses $m_n = \frac{n}{R}$. In other words, if the scalar field phi has a mass $m0$ in 4D, then the KK tower of this field in extra dimensions has a mass,

$$m^2 = m_0^2 + \frac{n_i^2}{R_i^2} + \cdots, \quad i = 5, 6, \ldots \tag{3.8}$$

where R_i denotes the size of the extra dimensions and n_i denotes the excitation levels. The size of the extra dimension must be sufficiently large to keep the masses small and within the extent of the accelerator energy in order to be able to observe such a KK tower.

3.1.1.2 Lagrangian of the MUED

The Lagrangian of the theory is obtained by embedding the 4-dimensional (4D) Standard Model Lagrangian into 5-dimensional (5D) geometry,

$$\begin{aligned}\mathcal{L}_{5D} = &-\frac{1}{4}G^a_{MN}G^{aMN} - \frac{1}{4}B_{MN}B^{MN} - \frac{1}{4}W^i_{MN}W^{iMN} + (D_M H)^\dagger \left(D^M H\right) \\ &+ i\bar{Q}\Gamma^M D_M Q + i\bar{L}\Gamma^M D_M L + i\bar{u}\Gamma^M D_M u + i\bar{d}\Gamma^M D_M d + i\bar{e}\Gamma^M D_M e \\ &+ \mu^2 H^\dagger H - \lambda_H \left(H^\dagger H\right)^2 - \left(y_u \bar{Q} u \widetilde{H} + y_d \bar{Q} d H + y_e \bar{L} e H + \text{ h.c. }\right)\end{aligned} \tag{3.9}$$

where B, W and G are U(1), SU(2) and SU(3) gauge bosons, respectively. L and Q are lepton and quark doublets, H and $\tilde{H}$ are Higgs fields where $\tilde{H} = i\sigma^2 H^*$. e, d and u represent the electron-like singlets, down-type and up-type quarks, respectively.

Γ^μ are the Dirac matrices $\Gamma^\mu = (\gamma^\mu, i\gamma^5)$ and the covariant derivative is,

$$D_M = \partial_M - iY g_1^{(5)} B_M - i g_2^{(5)} \frac{\sigma^i}{2} W_M^i - i g_3^{(5)} t^a G_M^a \tag{3.10}$$

where g_i are the 5D gauge couplings which are related to the couplings in the 4D by the relation $g_i^5 = g_i/\sqrt{\pi R}$, Y is the usual hypercharge, and t^a and σ^i are the Gell-Mann and Pauli matrices, respectively.

Decomposition of the Fields: In the Equation 3.7 kinetic term of a scalar field ϕ contains two derivatives, and it can be even or odd under a Z_2 transformation, i.e. $\phi(-y) = \pm\phi(y)$. Thus the expansion of a scalar field in KK modes is either,

$$\phi(x,y) = \frac{1}{\sqrt{\pi R}} \left[\phi^{(0)}(x) + \sqrt{2} \sum_{n=1}^{\infty} \phi^{(n)}(x) \cos \frac{ny}{R} \right], \quad \phi \text{ is even} \tag{3.11}$$

or,

$$\phi(x,y) = \sqrt{\frac{2}{\pi R}} \sum_{n=1}^{\infty} \phi^{(n)}(x) \sin \frac{ny}{R}, \quad \phi \text{ is odd} \tag{3.12}$$

It is convenient to represent a scalar field (such as the Higgs field) with an even scalar since it has a zero mode and is accompanied by the infinite tower of $\phi^{(n)}$ states.

A fermion field can be decomposed similarly. Higher dimensional fermions are placed on an orbifold S^1/Z_2 of length πR to produce 4D chiral fermions. Fermionic doublets and singlets are,

$$\begin{aligned} Q &= \frac{1}{\sqrt{\pi R}} \left\{ Q_L + \sqrt{2} \sum_{n=1}^{\infty} \left[Q_L^n \cos\left(\frac{ny}{R}\right) + Q_R^n \sin\left(\frac{ny}{R}\right) \right] \right\} \\ q &= \frac{1}{\sqrt{\pi R}} \left\{ q_R + \sqrt{2} \sum_{n=1}^{\infty} \left[q_R^n \cos\left(\frac{ny}{R}\right) + q_L^n \sin\left(\frac{ny}{R}\right) \right] \right\} \end{aligned} \tag{3.13}$$

Finally, the decomposition of a gauge boson A_μ is,

$$\begin{aligned} A_\mu(x,y) &= \frac{1}{\sqrt{\pi R}}\left[A_\mu^{(0)}(x) + \sqrt{2}\sum_{n=1}^{\infty} A_\mu^{(n)} \cos\frac{ny}{R}\right] \\ A_5(x,y) &= \sqrt{\frac{2}{\pi R}}\sum_{n=1}^{\infty} A_5^{(n)}(x) \sin\frac{ny}{R} \end{aligned} \tag{3.14}$$

Furthermore, the gauge can be chosen as $A_5 = 0$.

3.1.1.3 Interaction of Gravity with Matter

In the fat-brane model, gravity is assumed to propagate in the extra dimensions. The linearized metric field can be expanded over N large extra dimensions as,

$$\hat{h}_{\hat{\mu}\hat{\nu}}(x,y) = \sum_{\vec{n}} \hat{h}^{\vec{n}}_{\hat{\mu}\hat{\nu}}(x) \exp\left(i\frac{2\pi\vec{n}\cdot\vec{y}}{r}\right) \tag{3.15}$$

where $\hat{\mu},\hat{\nu} = 0,\ldots,3,\ldots 4+N$ and $\mu,\nu = 0,\ldots,3$.

The decomposition of $(4+N)D$ graviton field into a vector, scalar, and 4D tensor components is,

$$\hat{h}^{\vec{n}}_{\hat{\mu}\hat{\nu}} = V_N^{-1/2}\begin{pmatrix} h^{\vec{n}}_{\mu\nu} + \eta_{\mu\nu}\phi^{\vec{n}} & A^{\vec{n}}_{\mu i} \\ A^{\vec{n}}_{\nu j} & 2\phi^{\vec{n}}_{ij} \end{pmatrix} \tag{3.16}$$

where $i,j = 5,6,7,\cdots,4+N$, $\phi^{\vec{n}} = \phi^{\vec{n}}_{ii}$, and $V_N = r^N$ is the volume of the N-dimensional torus in which the large extra dimensions are compactified. Also, the three components of the $4+N$ dimensional tensor are ϕ_{ij}, $A_{\mu i}$ and $h_{\mu\nu}$ which are gravi-scalars, gravi-vectors and graviton, respectively. These three components are decomposed as in the Equation 3.16.

$$\begin{aligned}
\phi_{ij}(x,y) &= \sum_{\vec{n}} \phi_{ij}^{\vec{n}}(x) e^{i\frac{2\pi\vec{n}\cdot\vec{y}}{r}} \\
A_{\mu i}(x,y) &= \sum_{\vec{n}} A_{\mu i}^{\vec{n}}(x) e^{i\frac{2\pi\vec{n}\cdot\vec{y}}{r}} \\
h_{\mu\nu}(x,y) &= \sum_{\vec{n}} h_{\mu\nu}^{\vec{n}}(x) e^{i\frac{2\pi\vec{n}\cdot\vec{y}}{r}}
\end{aligned} \tag{3.17}$$

where $\vec{n} = \{n_1, n_2, \ldots, n_N\}$. $\vec{n} = 0$ modes corresponds to massless scalars, bosons, and gravitons in 4D, and $\vec{n} \neq 0$ is their higher level KK-states.

The following relations hold for the fields in Equation 3.17, and remove the extra internal degrees of freedom of the $4 + N$ dimensional graviton.

$$\partial^{\hat{\mu}} \left(\hat{h}_{\hat{\mu}\hat{\nu}} - \frac{1}{2} \hat{\eta}_{\hat{\mu}\hat{\nu}} \hat{h} \right) = 0, \quad n_i A_{\mu i}^{\vec{n}} = 0, \quad n_i \phi_{ij}^{\vec{n}} = 0 \tag{3.18}$$

Kinetic terms of the fields in Equations 3.11,3.13,3.14 have canonical form in the effective field theory. However, this is not true for the Lagrangian of the gravity written in terms of $\phi_{ij}^{\vec{n}}$, $A_{\mu i}^{\vec{n}}$, and $h_{\mu\nu}^{\vec{n}}$. Fields in the gravity Lagrangian will be redefined by using the relations in Equation 3.18, and physical fields $\widetilde{\phi}_{ij}^{\vec{n}}$, $\widetilde{A}_{\mu i}^{\vec{n}}$, and $\widetilde{h}_{\mu\nu}^{\vec{n}}$ will be introduced.

$$\begin{aligned}
h_{\mu\nu}^{\vec{n}} &= \widetilde{h}_{\mu\nu}^{\vec{n}} + \omega \left(\frac{\partial_\mu \partial_\nu}{m_{\vec{n}}^2} - \frac{1}{2} \eta_{\mu\nu} \right) \widetilde{\phi}^{\vec{n}} \\
A_{\mu i}^{\vec{n}} &= \widetilde{A}_{\mu i}^{\vec{n}} \\
\phi_{ij}^{\vec{n}} &= \frac{1}{\sqrt{2}} \widetilde{\phi}_{ij}^{\vec{n}} - \frac{3\omega a}{2} \left(\delta_{ij} - \frac{n_i n_j}{\vec{n}^2} \right) \widetilde{\phi}^{\vec{n}}
\end{aligned} \tag{3.19}$$

and $\phi^{\vec{n}} = (3\omega/2)\widetilde{\phi}^{\vec{n}}$.

The N-dimensional action describing the interaction of the matter with the gravity is,

$$\mathcal{S}_{int} = -\frac{\hat{\kappa}}{2} \int d^5x \delta\left(x^6\right) \ldots \delta\left(x^N\right) \hat{h}^{\hat{\mu}\hat{\nu}} T_{\hat{\mu}\hat{\nu}} \tag{3.20}$$

where $\hat{k}$ is the gravitational coupling in $4 + N$ dimension, and it is analogous to the 4D one by the relation $k = \hat{k} V_N^{-1/2}$, and $T_{\hat{\mu}\hat{\nu}}$ is the 5D energy-momentum tensor of

the matter.

Expand the gravity field in terms of KK-modes as,

$$\mathcal{S}_{\text{int}} = -\frac{\hat{\kappa}}{2}\int d^4x \int_0^{\pi R} dy \sum_{\vec{n}} \left[\left(h^{\vec{n}}_{\mu\nu} + \eta_{\mu\nu}\phi^{\vec{n}}\right) T_{\mu\nu} - 2A^{\vec{n}}_{\mu 5} T^{\mu}_{5} + 2\phi^{\vec{n}}_{55} T_{55}\right] e^{\frac{2\pi\imath(n_5 y)}{r}} \tag{3.21}$$

The effective 4D Lagrangian in terms of the physical fields is,

$$\begin{aligned}\mathcal{L}_{int} = -\frac{\kappa}{2}\sum_{\vec{n}}\Bigg\{ &\left[\widetilde{h}^{\vec{n}}_{\mu\nu} + \omega\left(\eta_{\mu\nu} + \frac{\partial_\mu\partial_\nu}{m^2_{\vec{n}}}\right)\widetilde{\phi}^{\vec{n}}\right] T^{\mu\nu}_{n_5} \\ &- 2\widetilde{A}^{\vec{n}}_{\mu 5} T^{\mu}_{n_5 5} + \left(\sqrt{2}\widetilde{\phi}^{\vec{n}}_{55} - \xi\widetilde{\phi}^{\vec{n}}\right) T^{n_5}_{55}\Bigg\}\end{aligned} \tag{3.22}$$

where the projections of the matter energy momantum tensor on the $\vec{n}$-th graviton state is defined as,

$$T^{n_5}_{MN}(x) = \int_0^{\pi R} dy T_{MN}(x,y) e^{2\pi i \frac{n_5 y}{r}} \tag{3.23}$$

From this Lagrangian, Feynman rules of the interaction of gravity with matter can be derived by using the explicit form of the energy-momentum tensor for each matter field [89].

3.2 Collider Phenomenology of Fat-Brane UED Model

In fat-brane UED scenarios, SM particles can reach a small ($R^{-1} \sim \ TeV$) extra dimension that extends through the large ($r^{-1} \sim (eV - keV)$) extra dimension which only gravity can reach. This orientation of the brane in bulk breaks the translational invariance at the small extra dimension, and the interactions preserve neither KK-parity nor KK-number. Violation of conservation of KK-parity and KK-number makes the collider phenomenology of fat-brane UED scenarios quite different from other UED models. For this reason, for example, level-1 KK particles can decay directly into SM particles and level-n gravitational excitation $G^{\vec{n}}$ ($G^{\vec{n}} \subset$ graviton,

gravi-vector and gravi- scalar) which has important implications for collider experiments. Examining the decay channels of the level-1 KK-particles in the fat-brane UED model would be convenient to observe these results.

3.2.1 Decay Channels of Level-1 KK Particles in Fat-Brane UED Model

There are two decay mechanisms for level-1 KK-particles from the fat-brane UED model. The first is the KKCD decays in the general UED models. Due to the conservation of KK-parity, heavier level-1 KK particles decay into SM particles and lighter level-1 KK particles. For example, the highest particle of the spectrum level-1 KK gluon g^1 decays into SM quarks and level-1 KK quarks (doublet Q^1 and singlet q^1) at almost the same rate. The only decay channels of singlet quarks are directly LKP (γ^1) and SM quarks, while doublet quarks Q^1 decay into level-1 electro-weak gauge bosons $W^{1\pm}$ / Z^1 and SM quark. The hadronic decay channels of level-1 gauge bosons are kinematically closed. Hence, they decay into SM leptons and level-1 KK leptons. Finally, decaying into SM lepton and LKP occurs. The LKP, not being stable in fat-brane model UED, further decays into γ/Z-boson and gravity excitation. Within this framework, the first type of collider signal expected by the model is $\gamma\gamma$, γZ or ZZ + X + missing E_T, where X in the expression corresponds to hadronic SM jets and/or leptons that cannot be observed in the detector. Another signal that can be considered under the same type of decay is γj + X + missing E_T. As details given in Figure 3.1 below, this final signal can be seen when both decay mechanisms (KKCD and GMD) contribute similarly. Another issue with KKCD decay widths is that these widths (as in mUED) depend only on R^{-1} and Λ and are independent of the number (N) or length (r) of the large extra dimensions.

Another type of decay specific to the fat-brane UED model is gravity-mediated decays. As discussed in the previous sections, neither KK-number nor KK-parity is a conservative symmetry under gravity-matter interactions. As a result, level-1 KK particles can decay directly into SM particle and $G^{\vec{n}} \subset$ (graviton, gravi-vector and gravi-scalar). Using Feynman rules derived from the action describing the gravity-matter interactions, the partial GMD decay width of level-1 KK-particles into level-n gravity excitation can be calculated, and total decay width can be obtained by summing

all possible decay amplitudes for all gravity excitations with masses smaller than the mass of the decaying particle. Thus, as a result of the gravity-matter interaction, level-1 KK particles (g^1, Q^1 and q^1) produced after the collision directly decay into SM jets and $G^{\vec{n}}$ resulting in di-jet and the missing transverse energy signal at parton level. Unlike KKCD, the GMD decay width directly depends on the large extra dimension number N and its length r.

Expected final signal from the model and how it will be observed depends on which decay channels have been described above will dominate the other. In order to examine this situation in more detail, it is helpful to examine how the decay mechanisms of level-1 KK gluons and quarks are affected in cases where $N = 2, 4, 6$, with the help of Figure 3.1, in which the decay widths of the particles have shown.

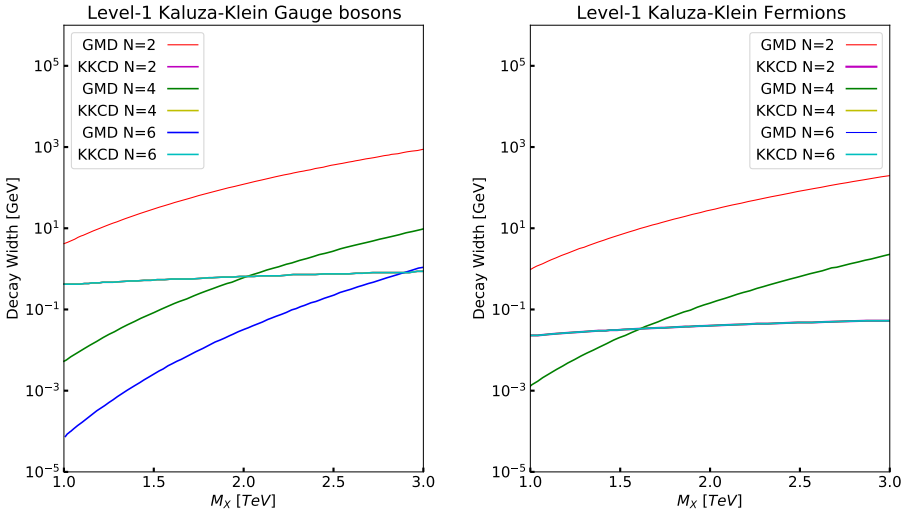

Figure 3.1: The Gravity Mediated Decay (GMD) and KK-Number Conserving Decay (KKCD) widths for level-1 quarks (right) and level-1 KK gauge boson (left) as a function of the mass of the particle M_X. N is the number of large extra dimensions. $R = 5$ and $M_D = 5$ TeV are set in producing KKCD and GMD widths [87].

For $N = 6$: In this particular case, GMD widths remain low compared to KKCD decay widths. As a result, the level-1 KK-particles decay into the lighter level-1 KK-particles and relevant SM particles in successive decays. The successive decay continues until LKP (γ_1). Contrary to the mUED model, the LKP is no longer stable and decays to photon and level-n gravity excitation ($G^{\vec{n}}$) via the GMD. For example,

considering that there are two decays per event, it can be said that the pairwise generation and decay of g^1 is characterized by $\gamma\gamma$ + lepton + jet and missing transverse energy. In this final signal, the source of the missing transverse energy is gravity excitation, while jets and leptons are released as a result of successive decay.

For $N = 2$ or $N = 4$: In this particular case, GMD widths are comparable to or higher than KKCD decay widths (Figure 3.1). For example, if N=2 case, for the level-1 KK particle in the mass range of $M_X = 1 - 3\ TeV$ shown in Figure 3.1, GMD is the dominant decay channel compared to KKCD. Likewise, for $N = 4$, it will be seen that GMD is the dominant decay channel for masses of $M_X \gtrsim 2, (1.5)$ TeV level-1 KK gauge bosons (fermions). For these reasons, when $N = 2$ and 4, successive decays of level-1 KK-particles may include decays with GMD and KKCD at each decay step.

In the light of the above discussions, in the fat-brane UED models, in addition to the $\gamma\gamma$ + missing transverse energy signal for the $N = 6$ state, especially in the $N = 2, 4$ states, after the direct decay of pair produced coloured level-1 KK-particles (gluons and quarks) into gravity excitation, multi-jet + missing transverse energy signal is expected. On the other hand, decomposition of one of the produced level-1 KK-particles via KKCD and the other via GMD to form the final signal γj plus missing transverse energy is also expected. After discussing the decay channels in the model and the final signals that may occur, the experimental studies (i) multi-jet and missing transverse energy (ii) γj plus missing transverse energy signals, which is examined within the scope of this thesis, will be discussed, and the state of the model under these current data will be examined then.

3.2.2 ATLAS Multi-jet and Missing Transverse Momentum Searches

The multi-jet and missing transverse energy final signal is a characteristic signal type that is expected from the SUSY models in which R-parity is conserved, resulting from the sequential decay of pair-produced squarks and gluinos, and is a type of signal topology that the leading groups in the LHC (ATLAS and CMS) often work. The most recent study of the ATLAS group on this signal can be found in [90]. In this study, the ATLAS collaboration used the total data of $139\ fb^{-1}$ integrated luminosity

at the centre of mass energy of $\sqrt{s} = 13\ TeV$ in the LHC and did not observe an event above the expected background event level from the SM, and 95% CL upper limits are set on R-parity conserved simplified SUSY model parameters (masses of SUSY particles). On the other hand, the model-independent 95% CL upper limits are set on the cross-section in the signal regions (SR) examined in the study mentioned above. These values can also be used to restrict the parameters of other models.

To make their analysis even more inclusive, the ATLAS group characterizes the multi-jet signal with increasing jet numbers and divides it into ten distinct signal regions. The analysis of the ATLAS group can be summarized in three parts:

Object reconstruction: Jet candidates were reconstructed within a jet radius parameter of $R = 0.4$ and anti-k_T jet clustering algorithm. From the regenerated jets, those that met the criteria $p_T^j \geq 20\ GeV$ and $|\eta^j| < 2.8$ were included in the further stages of the analysis. Electron (muon) candidates are required to meet the criteria $p_T^l > 7\,(6)\ GeV$ and $\left|\eta^l\right| \leq 2.47\,(2.7)$. Signal-region electrons and muons are then required to be isolated, satisfying a loose isolation requirement and having $p_T > 25GeV$. Then, leptons as close to the regenerated jets as $\Delta R < \min\left(0.4,\ 0.04 + \frac{10GeV}{p_T^{e\ /\mu}}\right)$ were excluded from the analysis. By using the remaining visible objects (jet, lepton, photon), the missing transverse energy E_T^{miss} in the event was computed with an object-based algorithm considering baseline objects. For the event with n_j jets, the effective mass parameter is defined as m_{eff}, defined as the scalar sum of the missing transverse energy and the energies of all jets satisfying the $p_T^j > 50\ GeV$ conditions. This parameter is very effective in distinguishing SUSY models containing heavy particles from SM background events. After reconstruction of the different physical objects (jets, leptons, photons, E_T^{miss}), the events were subjected to preselection criteria for further analysis.

Pre-selection criteria: Events satisfying the condition $\left|p_T^{j_1}\right| > 200\ GeV$ of the leading jet and the condition $\left|p_T^{j_2}\right| > 50\ GeV$ of at least one jet are selected for further analysis. Events containing leptons were excluded from the analysis (all events involving electron (muon) with $p_T > 7\,(6)\ GeV$ were rejected). It is ensured that the events in the analysis contain a relatively high degree of missing transverse energy of $E_T^{miss} > 300\ GeV$ and effective mass of $m_{eff} > 800\ GeV$. Events that do not

meet the criterion $\Delta\phi\left(j_{1,2}, p_T^{miss}\right)_{min} > 0.4$ ($\Delta\phi$ is angular separation between jet and p_T^{miss}) are excluded.

Event Selection and Signal Regions (SR): After the objects were defined and approved through the preselection criteria, ten different signal regions were defined, where the number of jets started from 2 and then increased to 6. The analysis has been comprehensive, with signal regions characterized by increasing jet numbers and m_{eff} values. Signal region definitions, preselection criteria and model-independent upper limits of cross sections ($\langle\epsilon\sigma\rangle_{obs}^{95}$) for each signal region at 95% CL reached by the ATLAS Collaboration is presented in Tables 3.1 and 3.2.

Table 3.1: Summary of common pre-selection criteria and signal regions used in the ATLAS Collaboration multi-jet and missing transverse energy signal search at a center of mass energy of $\sqrt{s} = 13$ TeV, corresponding to an integrated luminosity of $\mathcal{L} = 139\ fb^{-1}$ [90].

Cuts	Preselection Criteria		
$Electron\ [GeV]$	$p_T > 7$		
$Muon\ [GeV]$	$p_T > 6$		
E_T^{miss}[GeV]	> 300		
$p_T\ (j_1)\ [GeV]$	> 200		
$p_T\ (j_2)\ [GeV]$	> 50		
$\Delta\phi\left(j_{1,2,(3)}, \mathbf{p}_T^{miss}\right)_{min}$	> 0.2		
$m_{eff}\ [GeV]$	> 800		
	Signal Regions (SR)		
Cuts	2j-1600	2j-2200	2j-2800
N_j	≥ 2		
$p_T\ (j_1)\ [GeV]$	> 250	> 600	> 250
$\lvert p_T\left(j_{i=2,\ldots,N_{j_{min}}}\right)\ [GeV]\rvert$	> 250	> 50	> 250
$\lvert\eta\left(j_{i=1,\ldots,N_{j_{min}}}\right)\rvert$	< 2.0	< 2.8	< 1.2
$\Delta\phi\left(j_{1,2,(3)}, \mathbf{p}_T^{miss}\right)_{min}$	> 0.8	> 0.4	> 0.8
$\Delta\phi\left(j_{i>3}, \mathbf{p}_T^{miss}\right)_{min}$	> 0.4	> 0.2	> 0.4
$Aplanarity$	-		
$E_T^{miss}/\sqrt{H_T}\ GeV^{1/2}$	> 16		
$m_{eff}\ [GeV]$	> 1600	> 2200	> 2800
$\langle\epsilon\sigma\rangle_{obs}^{95}\ [fb]$	1.47	0.78	0.14

Table 3.2: Summary of common preselection criteria and signal regions used in the ATLAS Collaboration multi-jet and missing transverse energy signal search at a center of mass energy of $\sqrt{s} = 13$ TeV, corresponding to an integrated luminosity of $\mathcal{L} = 139\ fb^{-1}$ [90](continued).

	Signal Regions (SR)		
Cuts	4j-1000	4j-2200	4j-3400
N_j	≥ 4		
$p_T\left(j_1\right)\ [GeV]$	> 200		
$\lvert p_T\left(j_{i=2,\ldots,N_{j_{min}}}\right)$ [GeV]$\rvert$	> 100		
$\lvert\eta\left(j_{i=1,\ldots,N_{j_{min}}}\right)\rvert$	< 2.0		
$\Delta\phi\left(j_{1,2,(3)},\ bfp_T^{miss}\right)_{min}$	> 0.4		
$\Delta\phi\left(j_{i>3}, \mathbf{p}_T^{miss}\right)_{min}$	> 0.2		
$Aplanarity$	> 0.04		
$E_T^{miss}/\sqrt{H_T}\ GeV^{1/2}$	> 16		> 10
$m_{eff}\ [GeV]$	> 1000	> 2200	> 3400
$\langle\epsilon\sigma\rangle_{obs}^{95}\ [fb]$	0.52	0.14	0.04

	Signal Regions (SR)			
Cuts	5j-1600	6j-1000	6j-2000	6j-3400
N_j	≥ 2	≥ 4		
$p_T\left(j_1\right)\ [GeV]$	> 250	> 200		
$\lvert p_T\left(j_{i=2,\ldots,N_{j_{min}}}\right)\ [GeV]\rvert$	> 250	> 100		
$\lvert\eta\left(j_{i=1,\ldots,N_{j_{min}}}\right)\rvert$	< 2.0	< 2.0		
$\Delta\phi\left(j_{1,2,(3)}, \mathbf{p}_T^{miss}\right)_{min}$	> 0.8			
$\Delta\phi\left(j_{i>3}, \mathbf{p}_T^{miss}\right)_{min}$	> 0.4			
$Aplanarity$	-	> 0.04		
$E_T^{miss}/\sqrt{H_T}\ GeV^{1/2}$	> 16			> 10
$m_{eff}\ [GeV]$	> 1600	> 1000	> 2200	> 3400
$\langle\epsilon\sigma\rangle_{obs}^{95}\ [fb]$	1.47	0.52	0.14	0.04

3.2.3 ATLAS Photonic Signal Search

The ATLAS Collaboration [12] used a dataset at the centre of mass energy of $\sqrt{s} = 13\ TeV$ corresponding to an integrated luminosity of $139\ fb^{-1}$ when examining this signal, which includes photons, jets and missing transverse energy. The analysis examines the expected signals from the (General Gauge Mediation (GGM)) SUSY models. Similar object reconstruction criteria were used with multi-jet analysis; the final signal was required to contain one isolated photon, hadronic jet, and missing transverse energy. Three signal regions (SRL, SRM, and SRT) were determined after object reconstruction, preselection criteria, event selection and definition of the signal region. Signal regions, kinematical constraints/cuts, and model-independent upper limits of cross sections ($\langle \epsilon\sigma \rangle_{obs}^{95}$) for each signal region at 95% CL set by the ATLAS Collaboration are given in Table 3.3.

Table 3.3: The ATLAS Collaboration photon-jet and missing p_T selection criteria for SRL, SRM and SRH regions [12]

Cuts	Signal Regions		
	SRL	SRM	SRH
N_{photon}	≥ 1	≥ 1	≥ 1
$p_T^{leading-\gamma}\ [GeV]$	145	300	400
N_{lepton}	0	0	0
N_{jets}	≥ 5	≥ 5	≥ 3
$\Delta\phi\,(jet, E_T^{miss})$	0.4	0.4	0.4
$\Delta\phi\,(\gamma, E_T^{miss})$	0.4	0.4	0.4
$E_T^{miss}\ [GeV]$	250	300	600
$H_T\ [GeV]$	2000	1600	1600
R_T^4	0.90	0.90	-
$\langle \epsilon\sigma \rangle_{obs}^{95}\ [fb]$	0.030	0.018	0.054

3.2.4 Current Status of Fat-Brane Model Under the ATLAS Researches

3.2.4.1 Agreement of the Analysis

The multi-directional collision simulation software PYTHIA [91] is used to determine the state of the parameter space of the fat-brane UED model under current observational data. In order to determine the extent to which the exclusion values from the multi-jet (and photonic signal) analysis of the ATLAS group can constrain the model under consideration, the viability and applicability of the analysis code have to be tested.

In the multi-jet report, the ATLAS group presented the cut-flow information of the pair-production of the gulino of mass $m_{\widetilde{g}} = 2200\ GeV$ and its direct decay to the lightest neutralino of mass $m_{\widetilde{\chi_1^0}} = 600\ GeV$ at a centre of mass energy of 13 TeV in Table 17 of [92], in which they simulated and showed how kinematic constraints affect the generated events. To demonstrate the accuracy of the analysis code and constraints that are used in this study, the pair-production of gluinos of mass $m_{\widetilde{g}} = 2200\ GeV$ at a centre of mass energy of $13\ TeV$ and its direct decay to the lightest neutralino of mass $m_{\widetilde{\chi_1^0}} = 600\ GeV$ is performed. While performing this simulation, the information of the particles in the SUSY spectrum (mass information, decay channels) is produced in the SUSPECT [93] software and introduced them to PYTHIA via the SLHA [94, 95] file. The decays, showers and hadronization of the particles were also performed via PYTHIA, and the hadronic jets were reconstructed using the anti-kT [96] algorithm with the help of the FastJet [97] package. Throughout the analysis, the parton distribution function set NNPDF2.3LO [98] is used, which the ATLAS group also used for simulations. In order to show the reliability of the analysis code that has been written, the ATLAS group cut-flow table and the values obtained were presented in Table 3.4 in a comparative way.

After this stage, the GMD decays found in the model has integrated into the PYTHIA program to examine the parameter space of the fat-brane UED model under current data. When scanning the parameter space of the model, $20\ GeV$ interval in the $R^{-1} = [1,\ 3]\ TeV$ range and $250\ GeV$ interval in the $M_D = [5,\ 15]\ TeV$ has taken. For each parameter value, 500000 events have been generated in the PYTHIA

event generator and passed through the analysis program, whose reliability has been verified. The cross-section values of each model parameter have been calculated in each signal region (ten in multi-jet analysis and three in photonic signal analysis). Cross section values have been compared to the model-independent cross section values given in the last row of Tables 3.1,3.2, and 3.3 for each signal region at 95% CL. In the case of a value larger than the given cross-section, it is concluded that the corresponding model parameter has been excluded at 95% CL. These calculations have been repeated for the values $N = 2, 4, 6$. At its current state, this analysis has been one of the most comprehensive and up-to-date analyzes of the fat-brane UED model in the literature.

As a result of this study, the details of which are given above, it was found that the parameter space of the examined model was excluded under the results of ATLAS multi-jet and photonic final signals, as given in the Figure 3.2.

3.3 Exclusion Limits on Fat-Brane UED Model Parameters

The collider phenomenology of the fat-brane UED model depends on three parameters. These are the radius of the small extra dimension (R), the large extra dimension Planck mass (M_D) (or the large extra dimension length r equivalent to this parameter), and the number of large extra dimensions (N). R determines the mass order of the level-1 KK particles and, therefore, the production cross-section of these particles in the LHC. On the other hand, M_D and N determine the mass difference between the excited gravitons and hence the graviton states and the gravity-mediated decay amplitude. The collider phenomenology of the model at the LHC is determined by determining these three parameters.

In this thesis, the parameter space of the fat-brane UED model investigated under the multi-jet [90] and photonic [12] signals of ATLAS Collaboration at $\sqrt{s} = 13\ TeV$ centre of mass energy and $139\ fb^{-1}$ luminosity. As a result of this study, given in Figure 3.2, the three parameters of the fat-brane UED model have been constrained by using the upper limits of model-independent cross section obtained by ATLAS Collaboration at 95% CL.

Exclusion limits for $N = 2$: The most distinctive feature of fewer large extra dimensions in the model is that the mass difference between graviton excitations is small; in other words, the number densities are higher than in other cases. The corollary of this in collider physics is that the GMD amplitudes of level-1 KK gauge bosons and fermions dominate (almost) at every R-value relative to the KKCD amplitudes. The high-value GMD amplitude allows the coloured level-1 KK quarks and gluons produced in pairs in the LHC to decay directly into the SM particle (quark or gluon) and graviton excitation, thus generating the missing transverse energy signal from the di-jet and graviton. As given in Figure 3.2a, the region under $R^{-1} = 2.9\ TeV$ is excluded by the ATLAS multi-jet 2j-2800 signal area, and this exclusion is also independent of the value $M_D = [5, 15]\ TeV$ that has scanned. On the other hand, as a result of the ATLAS group photonic signal study, the $R^{-1} < 1780\,(2200)\ GeV$ region is excluded for $M_D = 5\,(15)\ TeV$ values. The reason why the photonic signal is not sensitive to low R^{-1} is because GMD (KKCD) widths increase (decrease) with increasing $M_D\,(R^{-1})$.

Exclusion limits for $N = 4$: In this case, both decay amplitudes can become comparable, and the result becomes evident in Figure 3.2b. As a result of low (high) M_D values dominating GMD (KKCD), different signals are sensitive to different and complementary parts of the model's parameter space. It is concluded that at $N = 4$ value, the $R^{-1} < 2840\,(2900)\ GeV$ region was excluded at $M_D = 5\,(15)\ TeV$ values of the model.

Exclusion limits for $N = 6$: For this particular N value, KKCD has higher values than GMD at large R^{-1} and the direct result of this is that in the successive decay of the produced level-1 particles, the decay continues until γ_1, and then the LKP decays into photons and gravitons, thus making the photon-containing signal topology more common. It is seen in Figure 3.2c that the exclusion from the photonic signal is more evident. Within the scope of this thesis, ATLAS results were found to exclude the region $R^{-1} < 2740\,(2900)\ GeV$ and $M_D = 5\,(15)\ TeV$ of the model at $N = 6$. Besides, it can be understood that the ATLAS multi-jet search has sensitivity only in the $M_D < 8\ TeV$ region of the model.

Table 3.4: Cut-flow table for 4j-1000 signal area. The values in the second column are taken from Table 17 of [92]. The values in the third column are from this study and are presented for comparison.

Selection	Gluino-pair production and its direct decay to lightest neutralino ($m_{\widetilde{g}} = 2200\ GeV$ and $m_{\widetilde{\chi_1^0}} = 600\ GeV$, $\sqrt{s} = 13\ TeV$)	
Requirements	Efficiency (%)	
	Table 17 [92]	Results from this analysis
Pre-selection + jet multiplication ≥ 2	100	100
jet multiplicaion ≥ 4	92.7	98.7
$\Delta\phi\left(jet_{1,2,(3)}, \mathbf{p}_T^{miss}\right)_{min} > 0.4$	77.6	82.9
$\Delta\phi\left(jet_i > 3, \mathbf{p}_T^{miss}\right)_{min} > 0.2$	69.1	73.3
$p_T\left(jet_4\right) > 100\ GeV$	61.3	62.9
$\lvert\eta\left(jet_{1,2,3,4}\right)\}\rvert > 2.0$	55.7	57.7
$Aplanarity > 0.04$	38.7	44.2
$E_T^{miss}/\sqrt{H_T} > 16\ GeV^{1/2}$	24.1	27.8
$m_eff > 1000\ GeV$	24.1	27.8

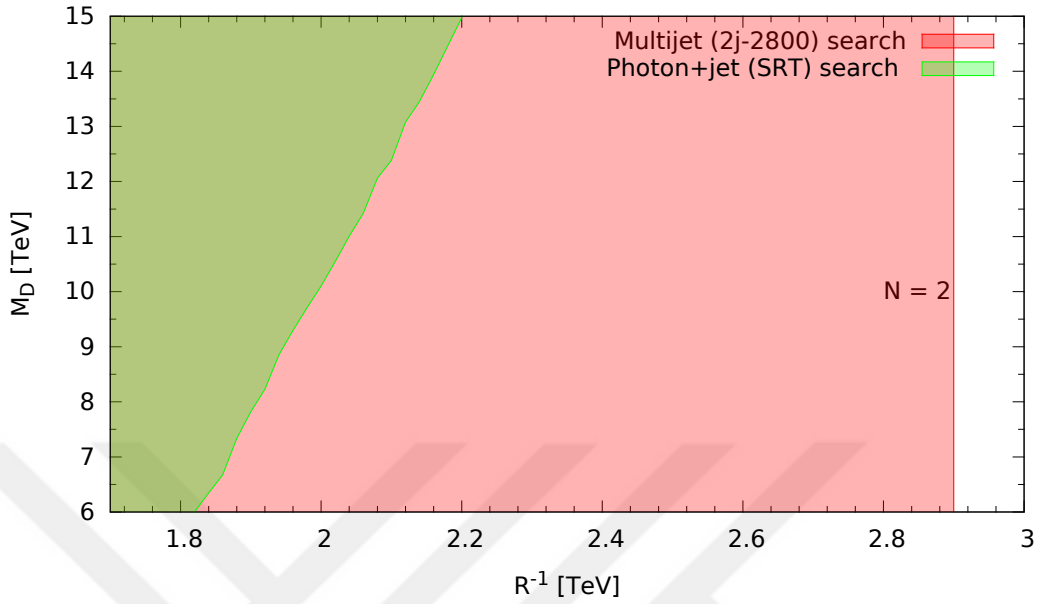

(a) 2j-1600 and SRT (photon + jet)

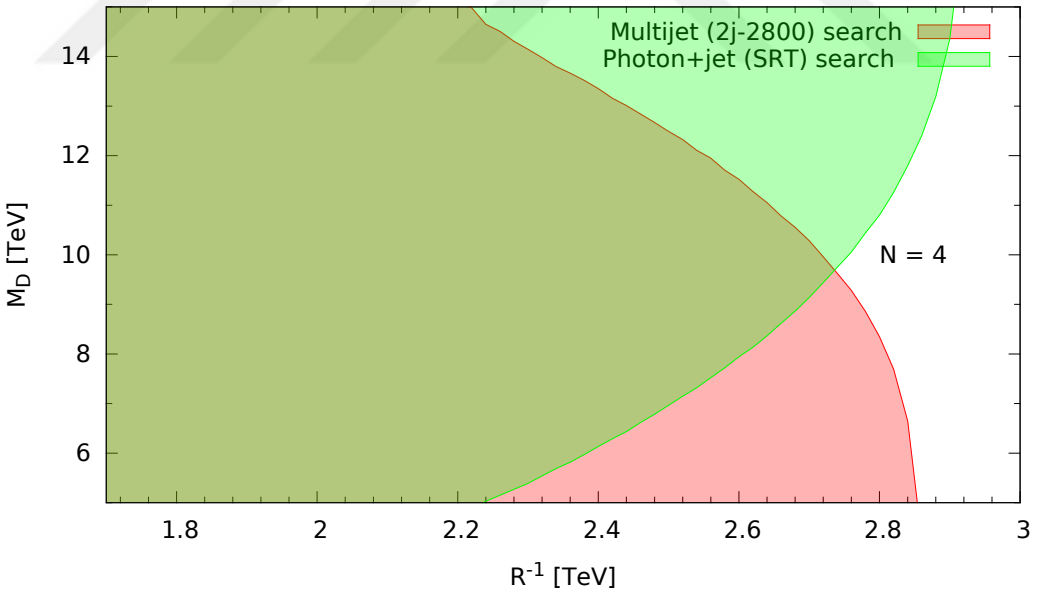

(b) 2j-2200 and SRT (photon + jet)

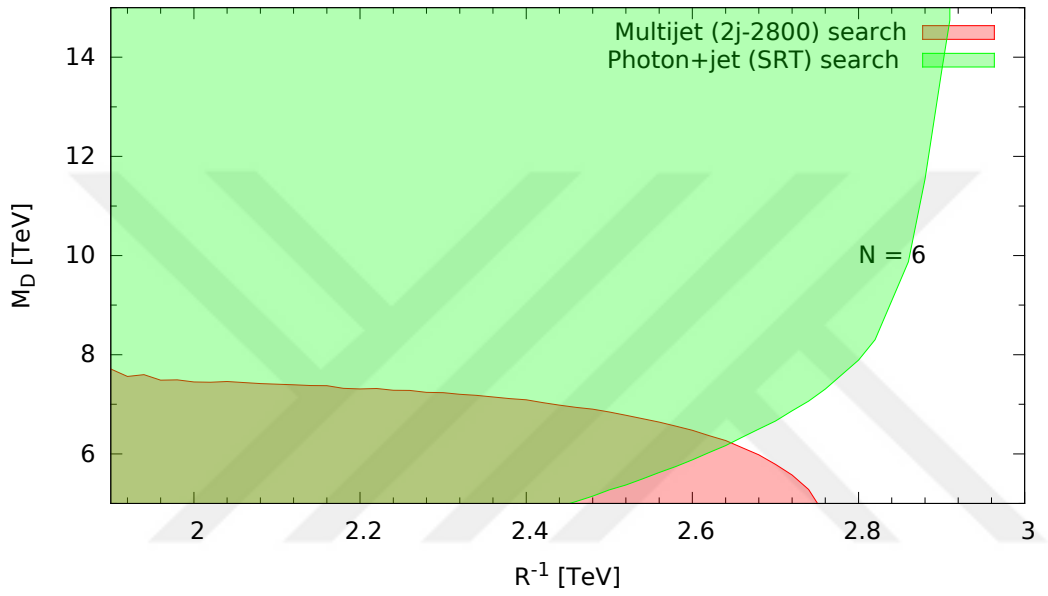

(c) 2j-2800 and SRT (photon + jet)

Figure 3.2: The exclusion regions of the fat-brane UED model parameters M_D and R^{-1} from ATLAS multi-jet (red) and γj (green) for $N = 6$. $\Lambda R^{-1} = 5$ is assumed throughout the analysis.

CHAPTER 4

CONCLUSIONS

It is known that the Standard Model is an effective theory valid up to energies around the electroweak scale. There is new physics which extends the validity of the Standard Model by embedding it into larger frameworks. The nature of new physics is a subject of intense studies. While it is common to assume that new physics lies beyond the Standard Model, it is equally possible to see signs of new physics in energies much less than the scale of the electroweak theory. Therefore, in this thesis, we have conducted a search for new physics extending in either side of the electroweak scale, namely the contribution of the dark photon to the charge radius of the neutrino and discerning signals of the fat-brane UED Model by using the LHC data.

In Chapter 2, two electromagnetic form factors of the neutrino which are the neutrino magnetic moment and the neutrino charge radius, are calculated in the $U_{B-L}(1)$ model. It is found that there is no contribution to the neutrino magnetic moment from the dark photon sector at one-loop level. On the other hand, it is shown that there is a finite contribution to the neutrino charge radius from the dark scenario at hand. Calculation of the electromagnetic vertex function responsible for the magnetic moment and charge radius has been carried out in a detailed manner. The one-loop integrals are handled with the help of publicly available Mathematica packages, FeynCalc [67, 68] and FeynArts [69]. Then, after the one-loop integrals are converted into the Passarino-Veltman functions, their explicit forms are obtained by taking the integrals with the help of the PackageX [70]. The non-trivial part of the calculation is the cancellation of the UV-divergent parts of the diagrams. Those parts from the proper vertex and self energy diagrams are extracted and it is found that, by using the t'Hooft-Feynman gauge, the total sum of these terms identically vanishes in the

$q^2 = 0$ limit. Therefore, it is concluded that the charge radius of the massive neutrino is a finite physical quantity. Furthermore, the validity of this assessment has been checked in the Standard Model limit (with the right-handed neutrinos added to the content of the SM) and are found to be in agreement with the previous calculations of the neutrino charge radius done by [66] where the gauge-independence and finiteness of the result has been shown explicitly in the $q^2 = 0$ limit by using general R_ξ gauge.

In future studies, analytical result obtained for the neutrino charge radius will be used to bound parameter space of the $U_{B-L}(1)$ model. The data from scattering experiments such as neutrino-electron scattering and coherent elastic neutrino nucleus scattering CEνNS can be used for this purpose since the diagrams of the charge radius also contribute to the scattering processes mentioned above which are expected to be sensitive to the light dark photon region.

In Chapter 3, new physics signals from the fat-brane UED model has been studied at the LHC. In the analyses carried out in this thesis, the parameter space of the fat-brane UED model in the range of $M_D = [5, 15]\ TeV$ and $R^{-1} = [1, 3]\ TeV$ are scanned for values $N = 2, 4, 6$ and some regions of the parameter space of the model are excluded with 95% CL on the ATLAS multi-jet and γj and missing transverse energy signals performed with the center of mass energy of $\sqrt{s} = 13TeV$ and $139\ fb^{-1}$ dataset. In addition to the di-photon plus missing transverse energy signal in the literature, it has also been shown that γj plus missing transverse energy signal can also constrain the parameters of the model. The current exclusions on the model have been improved by $\sim 200\ GeV$ for each $N = 2, 4, 6$ value at $M_D = 5\ TeV$ as a result of the multi-jet search. Similarly, in the context of constraints from the photon signal search, there is an improvement of $\sim 650\ GeV$ and $\sim 200\ GeV$ for $N = 2$ and $N = 4$ values at $M_D = 15\ TeV$, respectively. In the case of $N = 6$, the largest improvement is in the low M_D area, with $\sim 200\ GeV$ for $M_D = 5\ TeV$. No significant improvement has been seen at higher M_D values.

REFERENCES

[1] G. Aad, T. Abajyan, B. Abbott, *et al.*, "Observation of a new particle in the search for the standard model higgs boson with the atlas detector at the lhc," *Physics Letters, Section B: Nuclear, Elementary Particle and High-Energy Physics*, vol. 716, pp. 1–29, 2012.

[2] S. Chatrchyan, V. Khachatryan, A. M. Sirunyan, *et al.*, "Observation of a new boson at a mass of 125 gev with the cms experiment at the lhc," *Physics Letters, Section B: Nuclear, Elementary Particle and High-Energy Physics*, vol. 716, pp. 30–61, 2012.

[3] M. E. Peskin, *An Introduction To Quantum Field Theory*. CRC Press, 2018.

[4] "Standard Model Summary Plots March 2021," 2021.

[5] L. Susskind, "Dynamics of spontaneous symmetry breaking in the weinberg-salam theory," *Physical Review D*, vol. 20, pp. 2619–2625, 1979.

[6] V. F. Weisskopf, "On the self-energy and the electromagnetic field of the electron," *Physical Review*, vol. 56, pp. 72–85, 1939.

[7] K. G. Wilson, "Renormalization group and strong interactions," *Physical Review D*, vol. 3, pp. 1818–1846, 1971.

[8] K. A. O. et al, "Review of particle physics," *Chinese Physics C*, vol. 38, p. 090001, 2014.

[9] G. Bertone, D. Hooper, and J. Silk, "Particle dark matter: Evidence, candidates and constraints," *Physics Reports*, vol. 405, pp. 279–390, 2005.

[10] I. Antoniadis, N. Arkani-Hamed, S. Dimopoulos, and G. Dvali, "New dimensions at a millimeter to a fermi and superstrings at a tev," *Physics Letters, Section B: Nuclear, Elementary Particle and High-Energy Physics*, vol. 436, pp. 257–263, 1998.

[11] N. Arkani-Hamed, S. Dimopoulos, and G. Dvali, "The hierarchy problem and new dimensions at a millimeter," *Physics Letters, Section B: Nuclear, Elementary Particle and High-Energy Physics*, vol. 429, pp. 263–272, 1998.

[12] G. Aad, B. Abbott, D. C. Abbott, *et al.*, "Search for new phenomena in events with an energetic jet and missing transverse momentum in pp collisions at s =13 tev with the atlas detector," *Physical Review D*, vol. 103, p. 112006, 2021.

[13] L. Randall and R. Sundrum, "An alternative to compactification," 1999.

[14] L. Randall and R. Sundrum, "Large mass hierarchy from a small extra dimension," *Physical Review Letters*, vol. 83, pp. 3370–3373, 1999.

[15] G. Aad, B. Abbott, D. C. Abbott, *et al.*, "Search for resonances decaying into photon pairs in 139 fb^{-1} of pp collisions at $s = 13$ tev with the atlas detector," *Physics Letters B*, vol. 822, p. 136651, 2021.

[16] I. Antoniadis, "A possible new dimension at a few tev," *Physics Letters B*, vol. 246, pp. 377–384, 1990.

[17] T. Appelquist, "Bounds on universal extra dimensions," *Physical Review D*, vol. 64, 2001.

[18] H. C. Cheng, K. T. Matchev, and M. Schmaltz, "Radiative corrections to kaluza-klein masses," *Physical Review D*, vol. 66, 2002.

[19] G. Bhattacharyya, S. K. Majee, and A. Raychaudhuri, "Extra-dimensional relaxation of the upper limit of the lightest supersymmetric neutral higgs mass," *Nuclear Physics B*, vol. 793, pp. 114–130, 2008.

[20] G. Bhattacharyya, A. Datta, S. K. Majee, and A. Raychaudhuri, "Power law scaling in universal extra dimension scenarios," *Nuclear Physics B*, vol. 760, pp. 117–127, 2007.

[21] K. R. Dienes, E. Dudas, and T. Gherghetta, "Extra spacetime dimensions and unification," *Physics Letters, Section B: Nuclear, Elementary Particle and High-Energy Physics*, vol. 436, pp. 55–65, 1998.

[22] K. R. Dienes, E. Dudas, and T. Gherghetta, "Grand unification at intermediate mass scales through extra dimensions," *Nuclear Physics B*, vol. 537, pp. 47–108, 1999.

[23] S. Hossenfelder, "Running coupling with minimal length," *Physical Review D - Particles, Fields, Gravitation and Cosmology*, vol. 70, p. 11, 2004.

[24] N. Arkani-Hamed and M. Schmaltz, "Hierarchies without symmetries from extra dimensions," *Physical Review D - Particles, Fields, Gravitation and Cosmology*, vol. 61, 2000.

[25] B. A. Dobrescu and E. Poppitz, "Number of fermion generations derived from anomaly cancellation," *Physical Review Letters*, vol. 87, pp. 318011–318014, 2001.

[26] M. T. Arun, D. Choudhury, and D. Sachdeva, "Living orthogonally: quasi-universal extra dimensions," *Journal of High Energy Physics*, vol. 2019, 2019.

[27] G. Bélanger, M. Kakizaki, and A. Pukhov, "Dark matter in ued: The role of the second kk level," *Journal of Cosmology and Astroparticle Physics*, vol. 2011, p. 009, 2011.

[28] F. Burnell and G. D. Kribs, "The abundance of kaluza-klein dark matter with coannihilation," *Physical Review D - Particles, Fields, Gravitation and Cosmology*, vol. 73, 2006.

[29] H. C. Cheng, J. L. Feng, and K. T. Matchev, "Kaluza-klein dark matter," *Physical Review Letters*, vol. 89, 2002.

[30] J. M. Cornell, S. Profumo, and W. Shepherd, "Dark matter in minimal universal extra dimensions with a stable vacuum and the "right" higgs boson," *Physical Review D - Particles, Fields, Gravitation and Cosmology*, vol. 89, 2014.

[31] B. A. Dobrescu, D. Hooper, K. Kong, and R. Mahbubani, "Spinless photon dark matter from two universal extra dimensions," *Journal of Cosmology and Astroparticle Physics*, 2007.

[32] T. Flacke, D. W. Kang, K. Kong, *et al.*, "Electroweak kaluza-klein dark matter," *Journal of High Energy Physics*, vol. 2017, 2017.

[33] D. Hooper and S. Profumo, "Dark matter and collider phenomenology of universal extra dimensions," *Physics Reports*, vol. 453, pp. 29–115, 2007.

[34] Y. Ishigure, M. Kakizaki, and A. Santa, "Thermal relic abundance of the lightest kaluza-klein particle in phenomenological universal extra dimension models," 2016.

[35] M. Kakizaki, S. Matsumoto, and M. Senami, "Relic abundance of dark matter in the minimal universal extra dimension model," *Physical Review D - Particles, Fields, Gravitation and Cosmology*, vol. 74, 2006.

[36] K. Kong and K. T. Matchev, "Precise calculation of the relic density of kaluza-klein dark matter in universal extra dimensions," *Journal of High Energy Physics*, vol. 01, pp. 931–972, 2006.

[37] G. Servant and T. M. Tait, "Is the lightest kaluza-klein particle a viable dark matter candidate?," *Nuclear Physics B*, vol. 650, pp. 391–419, 2003.

[38] H.-C. Cheng, K. T. Matchev, and M. Schmaltz, "Bosonic supersymmetry? getting fooled at the cern lhc," *Phys. Rev. D*, vol. 66, p. 056006, 2002.

[39] W. Marciano and A. Sanda, "Exotic decays of the muon and heavy leptons in gauge theories," *Physics Letters B*, vol. 67, no. 3, pp. 303–305, 1977.

[40] B. W. Lee and R. E. Shrock, "Natural suppression of symmetry violation in gauge theories: Muon- and electron-lepton-number nonconservation," *Physical Review D*, vol. 16, pp. 1444–1473, 1977.

[41] K. Fujikawa and R. E. Shrock, "Magnetic moment of a massive neutrino and neutrino-spin rotation," *Physical Review Letters*, vol. 45, pp. 963–966, 1980.

[42] P. B. Pal and L. Wolfenstein, "Radiative decays of massive neutrinos," *Phys. Rev. D*, vol. 25, pp. 766–773, 1982.

[43] R. E. Shrock, "Electromagnetic properties and decays of dirac and majorana neutrinos in a general class of gauge theories," *Nuclear Physics, Section B*, vol. 206, pp. 359–379, 1982.

[44] S. M. Bilenky and S. T. Petcov, "Massive neutrinos and neutrino oscillations," *Rev. Mod. Phys.*, vol. 59, pp. 671–754, 1987.

[45] N. F. Bell, V. Cirigliano, M. J. Ramsey-Musolf, *et al.*, "How magnetic is the dirac neutrino?," *Phys. Rev. Lett.*, vol. 95, p. 151802, 2005.

[46] N. F. Bell, M. Gorchtein, M. J. Ramsey-Musolf, *et al.*, "Model independent bounds on magnetic moments of majorana neutrinos," *Physics Letters, Section B: Nuclear, Elementary Particle and High-Energy Physics*, vol. 642, pp. 377–383, 2006.

[47] G. G. Raffelt, "New bound on neutrino dipole moments from globular-cluster stars," *Phys. Rev. Lett.*, vol. 64, pp. 2856–2858, 1990.

[48] G. G. Raffelt, "Astrophysics probes of particle physics," *Physics Reports*, vol. 333-334, pp. 593–618, 2000.

[49] N. Viaux, M. Catelan, P. B. Stetson, *et al.*, "Particle-physics constraints from the globular cluster m5: Neutrino dipole moments," *Astronomy and Astrophysics*, vol. 558, 2013.

[50] W. Bardeen, R. Gastmans, and B. Lautrup, "Static quantities in weinberg's model of weak and electromagnetic interactions," *Nuclear Physics B*, vol. 46, no. 1, pp. 319–331, 1972.

[51] M. S. Dvornikov and A. I. Studenikin, "Electromagnetic form factors of a massive neutrino," *Journal of Experimental and Theoretical Physics*, vol. 99, no. 2, pp. 254–269, 2004.

[52] S. Y. Lee, "Higher-order corrections to leptonic processes and the renormalization of weinberg's theory of weak interactions in the unitary gauge," *Phys. Rev. D*, vol. 6, pp. 1701–1717, 1972.

[53] J. L. L. Martínez, A. Rosado, and A. Zepeda, "Neutrino charge in the linear R_ξ gauge," *Phys. Rev. D*, vol. 29, pp. 1539–1541, 1984.

[54] J. L. Lucio, A. Rosado, and A. Zepeda, "Characteristic size for the neutrino," *Phys. Rev. D*, vol. 31, pp. 1091–1096, 1985.

[55] G. Degrassi, A. Sirlin, and W. J. Marciano, "Effective electromagnetic form factor of the neutrino," *Phys. Rev. D*, vol. 39, pp. 287–294, 1989.

[56] J. Bernabé u, L. Cabral-Rosetti, J. Papavassiliou, and J. Vidal, “Charge radius of the neutrino,” *Physical Review D*, vol. 62, no. 11, 2000.

[57] J. Bernabé u, J. Papavassiliou, and J. Vidal, “Observability of the neutrino charge radius,” *Physical Review Letters*, vol. 89, no. 10, 2002.

[58] J. Bernabéu, J. Papavassiliou, and J. Vidal, “The neutrino charge radius as a physical observable,” *Nuclear Physics B*, vol. 680, no. 1-3, pp. 450–478, 2004.

[59] K. Fujikawa and R. Shrock, “Comment on "observability of the neutrino charge radius",” 2003.

[60] K. Fujikawa and R. Shrock, “Neutrino electroweak radius,” *Physical Review D*, vol. 69, no. 1, 2004.

[61] J. Papavassiliou, J. Bernabéu, D. Binosi, and J. Vidal, “The effective neutrino charge radius,” *The European Physical Journal C*, vol. 33, no. S1, pp. s865–s867, 2003.

[62] D. Binosi, J. Bernabéu, and J. Papavassiliou, “The effective neutrino charge radius in the presence of fermion masses,” *Nuclear Physics B*, vol. 716, no. 1, pp. 352–372, 2005.

[63] B. Holdom, “Two u(1)’s and epsilon charge shifts,” *Physics Letters B*, vol. 166, pp. 196–198, 1986.

[64] M. Pospelov, “Secluded u(1) below the weak scale,” 2009.

[65] M. Cirelli, P. Panci, K. Petraki, *et al.*, “Dark matter’s secret liaisons: phenomenology of a dark u(1) sector with bound states,” *Journal of Cosmology and Astroparticle Physics*, vol. 2017, pp. 036–036, 2017.

[66] M. Dvornikov and A. Studenikin, “Electric charge and magnetic moment of a massive neutrino,” *Physical Review D*, vol. 69, no. 7, 2004.

[67] R. Mertig, M. Böhm, and A. Denner, “Feyn calc - computer-algebraic calculation of feynman amplitudes,” *Computer Physics Communications*, vol. 64, no. 3, pp. 345–359, 1991.

[68] V. Shtabovenko, R. Mertig, and F. Orellana, "FeynCalc 9.3: New features and improvements," *Computer Physics Communications*, vol. 256, p. 107478, 2020.

[69] T. Hahn, "Generating feynman diagrams and amplitudes with FeynArts 3," *Computer Physics Communications*, vol. 140, no. 3, pp. 418–431, 2001.

[70] H. H. Patel, "Package-x: A mathematica package for the analytic calculation of one-loop integrals," *Computer Physics Communications*, vol. 197, pp. 276–290, 2015.

[71] B. Bhattacherjee and K. Ghosh, "Search for the minimal universal extra dimension model at the lhc with $s = 7$ TeV," *Physical Review D - Particles, Fields, Gravitation and Cosmology*, vol. 83, 2011.

[72] G. Cacciapaglia, A. Deandrea, J. Ellis, *et al.*, "Lhc missing-transverse-energy constraints on models with universal extra dimensions," *Physical Review D - Particles, Fields, Gravitation and Cosmology*, vol. 87, 2013.

[73] A. Datta, A. Datta, and S. Poddar, "Enriching the exploration of the mued model with event shape variables at the cern lhc," *Physics Letters, Section B: Nuclear, Elementary Particle and High-Energy Physics*, vol. 712, pp. 219–225, 2012.

[74] T. G. Rizzo, "Probes of universal extra dimensions at colliders," *Physical Review D - Particles, Fields, Gravitation and Cosmology*, vol. 64, pp. 950101–950109, 2001.

[75] G. Servant, "Status report on universal extra dimensions after lhc8," *Modern Physics Letters A*, vol. 30, 2015.

[76] A. Datta, G. L. Kane, and M. Toharia, "Is it susy?," 2005.

[77] A. K. Datta, K. Kong, and K. T. Matchev, "Discrimination of supersymmetry and universal extra dimensions at hadron colliders," *Physical Review D - Particles, Fields, Gravitation and Cosmology*, vol. 72, 2005.

[78] A. Datta, K. Kong, and K. T. Matchev, "Erratum: Discrimination of supersymmetry and universal extra dimensions at hadron colliders (physical review d - particles, fields, gravitation and cosmology (2005) 72 (096006))," *Physical Review D - Particles, Fields, Gravitation and Cosmology*, vol. 72, 2005.

[79] I. Antoniadis, K. Benakliand, and M. Quirós, "Direct collider signatures of large extra dimensions," *Physics Letters, Section B: Nuclear, Elementary Particle and High-Energy Physics*, vol. 460, pp. 176–183, 1999.

[80] A. D. Rújula, A. Donini, M. B. Gavela, and S. Rigolin, "Fat brane phenomena," *Physics Letters, Section B: Nuclear, Elementary Particle and High-Energy Physics*, vol. 482, pp. 195–204, 2000.

[81] D. A. Dicus, C. D. McMullent, and S. Nandi, "Collider implications of kaluza-klein excitations of the gluons," *Physical Review D - Particles, Fields, Gravitation and Cosmology*, vol. 65, pp. 760071–7600719, 2002.

[82] A. Donini and S. Rigolin, "Anisotropic type i string compactification, winding modes and large extra dimensions," *Nuclear Physics B*, vol. 550, pp. 59–76, 1999.

[83] E. Gabrielli and B. Mele, "Gravitational decays of heavy particles in large extra dimensions," *Nuclear Physics B*, vol. 647, pp. 319–343, 2002.

[84] C. Macesanu, C. D. McMullen, and S. Nandi, "New signal for universal extra dimensions," *Physics Letters, Section B: Nuclear, Elementary Particle and High-Energy Physics*, vol. 546, pp. 253–260, 2002.

[85] C. Macesanu, S. Nandi, and M. Rujoiu, "Single kaluza-klein production in universal extra dimensions," *Physical Review D - Particles, Fields, Gravitation and Cosmology*, vol. 71, p. 036003, 2005.

[86] C. Macesanu, S. Nandi, and M. Rujoiu, "Monojet and single photon signals from universal extra dimensions," *Physical Review D*, vol. 73, p. 076001, 2006.

[87] K. Ghosh, D. Karabacak, and S. Nandi, "Universal extra dimension models with gravity mediated decays after lhc run ii data," *Physics Letters, Section B: Nuclear, Elementary Particle and High-Energy Physics*, vol. 788, pp. 388–395, 2019.

[88] K. Ghosh and K. Huitu, "Constraints on universal extra dimension models with gravity mediated decays from atlas diphoton search," *Journal of High Energy Physics*, vol. 2012, pp. 1–24, 2012.

[89] C. Macesanu, A. Mitov, and S. Nandi, "Gravity and matter in extra dimensions," 2003.

[90] G. Aad, B. Abbott, D. C. Abbott, *et al.*, "Search for squarks and gluinos in final states with jets and missing transverse momentum using $139\ fb^{-1}$ of $s = 13$ TeV pp collision data with the atlas detector," *Journal of High Energy Physics*, vol. 2021, pp. 1–64, 2021.

[91] T. Sjöstrand, P. Edén, C. Friberg, *et al.*, "High-energy-physics event generation with pythia 6.1," *Computer Physics Communications*, vol. 135, pp. 238–259, 2001.

[92] "Search for squarks and gluinos in final states with jets and missing transverse momentum using 139 fb^{-1} of $\sqrt{s}$ =13 TeV pp collision data with the ATLAS detector," 2019. All figures including auxiliary figures are available at https://atlas.web.cern.ch/Atlas/GROUPS/PHYSICS/CONFNOTES/ATLAS-CONF-2019-040.

[93] A. Djouadi, J.-L. Kneur, and G. Moultaka, "Suspect: A fortran code for the supersymmetric and higgs particle spectrum in the mssm," *Computer Physics Communications*, vol. 176, pp. 426–455, 2007.

[94] B. C. Allanach, C. Balázs, G. Bélanger, *et al.*, "Susy les houches accord 2," *Computer Physics Communications*, vol. 180, pp. 8–25, 2009.

[95] P. Skands, B. C. Allanach, H. Baer, *et al.*, "Susy les houches accord: Interfacing susy spectrum calculators, decay packages, and event generators," *Journal of High Energy Physics*, vol. 8, pp. 851–881, 2004.

[96] M. Cacciari, G. P. Salam, and G. Soyez, "The anti-k t jet clustering algorithm," *Journal of High Energy Physics*, vol. 2008, p. 63, 2008.

[97] M. Cacciari, G. P. Salam, and G. Soyez, "Fastjet user manual: (for version 3.0.2)," *European Physical Journal C*, vol. 72, pp. 1–54, 2012.

[98] T. N. Collaboration, R. D. Ball, V. Bertone, *et al.*, "Parton distributions for the lhc run ii," *Journal of High Energy Physics*, vol. 2015, pp. 1–148, 2014.